Neurobiology of Disease 220 (2026) 107304

Contents lists available at ScienceDirect

Neurobiology of Disease

journal homepage: www.elsevier.com/locate/ynbdi

Hippocampal glial alterations are associated with Lamin B1 dysregulation and abnormal nuclear morphology in a rat model of fragile X syndrome

Alessandro Rava [a,b,1], Alessandro Feo [a,1], Giulia Bagnato [c], Valentina D'Oria [d], Marco Pezzullo [d], Stefania Petrini [d], Valeria Buzzelli [a], Fabrizio Ascone [a], Melania Di Trapano [a], Barbara Peruzzi [e,f,**,2], Viviana Trezza [a,b,*,2]

[a] Dept. Science, Roma Tre University, Rome, Italy
[b] Neuroendocrinology, Metabolism and Neuropharmacology Unit, IRCCS Fondazione Santa Lucia, Rome, Italy
[c] DAHFMO - Section of Histology and Medical Embryology, University of Rome Sapienza, Rome, Italy
[d] Core Facilities, Bambino Gesù Children Hospital IRCCS, Rome, Italy
[e] Dept. of Life Science and Public Health, Section of Histology and Embryology, Catholic University of Sacred Heart, Rome, Italy
[f] Oncology and Experimental Neuroscience Unit, IRCCS Fondazione Policlinico "Agostino Gemelli", Rome, Italy

ARTICLE INFO

Keywords:
ASD
FXS
hippocampus
Glia
Lamin B1
Nuclei

ABSTRACT

Fragile X syndrome (FXS) is the most common inherited intellectual disability and the leading monogenic cause of autism spectrum disorders (ASD). Although the pathological mechanisms underlying this neurodevelopmental disorder are challenging, recent studies have increasingly highlighted the involvement of glial cells in the pathogenesis of both ASD and FXS. Microglia and astrocytes are critical for brain development and homeostasis; thus, understanding glial dysfunction in both the developing and adult brain in these disorders may reveal novel therapeutic targets beyond the neuro-centric perspective. In this study, we demonstrated that the loss of function of Fmrp leads to phenotypic changes in both microglia and astrocytes within the hippocampus of the recently validated *Fmr1-$^{\Delta}$exon 8* rat model of FXS without a significant induction of pro-inflammatory cytokines. For the first time, we also provide evidence that these non-inflammatory changes in glia are associated with dysmorphic nuclei and a reduced expression of Lamin B1, a key component of the nuclear envelope and an important modulator of brain development and aging, in the hippocampus of young adult *Fmr1-$^{\Delta}$exon 8* rats.

Collectively, our findings strengthen existing evidence of the glial contribution to FXS and identify Lamin B1 loss and nuclear abnormalities as potential early markers of hippocampal pathology, providing a novel potential molecular target which should be furtherly considered.

1. Introduction

Fragile X syndrome (FXS) is the most common inherited form of intellectual disability and the leading monogenic cause of autism spectrum disorders (ASD). It is caused by the silencing of the Fragile X Messenger Ribonucleoprotein 1 (*Fmr1*) gene, which encodes the Fragile X Messenger Ribonucleoprotein (FMRP), an RNA-binding protein regulating the translation of a broad set of mRNAs involved in multiple biological processes, including neurotransmission and synaptic plasticity (Genovese and Butler, 2025). Accordingly, individuals with FXS show specific neurodevelopmental, behavioral, and psychiatric conditions over the lifespan (Genovese and Butler, 2025). Numerous compounds have been tested over the years to rescue or mitigate FXS symptoms. However, clinical trials have often failed to demonstrate efficacy (Berry-Kravis et al., 2018), highlighting the urgent need to understand the molecular mechanisms driving the pathogenesis of FXS.

* Corresponding author at: Department of Science, Section of Biomedical Sciences and Technologies, Roma Tre University, Viale G. Marconi 446, 00146 Rome, Italy.
** Corresponding author at: Department of Life Science and Public Health, Section of Histology and Embryology, Catholic University of Sacred Heart, Largo Francesco Vito 1, 00168 Rome, Italy.
E-mail addresses: barbara.peruzzi@unicatt.it (B. Peruzzi), viviana.trezza@uniroma3.it (V. Trezza).
[1] Shared first authorship.
[2] Shared last authorship.

https://doi.org/10.1016/j.nbd.2026.107304
Received 24 November 2025; Received in revised form 30 January 2026; Accepted 1 February 2026
Available online 4 February 2026

Although the pathological mechanisms underlying this neurodevelopmental disorder are complex, clinical and preclinical evidence suggests that glial cell alterations contribute to the pathophysiology of FXS and ASD-related disorders (Hughes et al., 2023; Napier et al., 2023; Talvio and Castren, 2023). Indeed, FMRP is also expressed in non-neuronal cells, including astrocytes (Pacey and Doering, 2007) and microglia (D'Antoni et al., 2024; Gholizadeh et al., 2015). Glial cells play an essential role in brain development and function, including neurogenesis, neuronal migration, synaptic patterning, neurotransmission, immune response and aging (Allen and Lyons, 2018; Gildea and Liddelow, 2025; Lopez-Ortiz and Eyo, 2024). Therefore, the loss of FMRP in these cells may disrupt developmental trajectories and adult brain homeostasis, increasing the susceptibility to ASD and FXS-like phenotypes.

Interestingly, recent evidence suggests nuclear lamins as pivotal modulators of brain development and aging, and lamin defects have recently been associated with glial dysfunction in age-related brain disorders, including Alzheimer's disease, Autosomal Dominant Leukodystrophy, and Parkinson's disease (Koufi et al., 2023).

Lamins are the major components of the nuclear envelope and play crucial roles as mechanosensitive proteins in the structural and functional integrity of the nucleus along with the organization of the cytoskeleton, DNA regulation, control of cell proliferation and survival, and mechanotransduction (de Leeuw et al., 2018; Sun et al., 2025; Vahabikashi et al., 2022). The expression of each lamin subtype is regulated in tissue-specific, as well as cell-type specific manners (Broers et al., 1997), and mainly driven by signals of mechanical nature, among which the tissue-specific elasticity (Swift et al., 2013). Although ubiquitously expressed, B-type lamins (especially the isoform B1) are the only lamins consistently detected in all neural cells in the rat cerebral cortex (Takamori et al., 2018), as A-type lamins are poorly expressed in soft tissues (Swift et al., 2013). Interestingly, FXS patients and *Fmr1*-KO mice exhibiting cognitive impairments, also show abnormal hippocampal size and connectivity (Haberl et al., 2015; Kates et al., 1997; Molnar and Keri, 2014), thereby suggesting a mechanical aberration in the brain environment that could be related to lamin deregulation. In support of this hypothesis, higher Matrix Metalloproteinase-9 (MMP-9) activity in *Fmr1*-KO mouse brains has been reported, suggesting that MMP-9 dysregulation may contribute to FXS-associated deficits (Bilousova et al., 2009). Since MMP-9 activity has an effect on the processing of extracellular matrix as well as proper function of adhesion molecules (Dziembowska and Wlodarczyk, 2012), increased MMP-9 levels in FXS can partially explain the altered extracellular matrix elasticity and plasticity observed in the *Fmr1*-KO animal model (Zhang et al., 2009). Moreover, abnormal Lamin B1 expression has been previously associated with diseases mainly affecting the brain, where Lamin B1 expression is finely tuned to properly regulate key cell processes, such as neuronal migration, neurogenesis, cell differentiation, and senescence both during development and aging (Koufi et al., 2023). Therefore, given the emerging role of Lamin B1 in regulating glial function under pathophysiological conditions and the altered mechano-environment described in animal models of FXS, it is plausible that Lamin B1 dysregulation may contribute to the altered glial phenotypes observed in FXS and ASD-related disorders. On this basis, the aim of this study was to investigate whether astrocytic and microglial alterations in the hippocampus - a central area for learning and memory, and significantly impacted by the loss of FMRP (Bostrom et al., 2016; Long et al., 2024) - correlate with a decline in Lamin B1 expression and defective nuclear morphology in the *Fmr1-*$^{\Delta}$*exon 8* rat model, which has been proposed as a genetic rat model relevant to FXS and ASD (Golden et al., 2019). This model was generated using zinc-finger nucleases (ZFN) and carries a deletion of exon 8 of the *Fmr1* gene, which encodes the KH1 RNA-binding domain of FMRP. Although this mutation differs from the full knockout observed in most individuals with FXS, deletion of exon 8 has been reported to be sufficient to induce FXS-like traits, including deficits in sustained visuospatial attention, altered social interactions, impairments in working memory, and abnormal synaptic plasticity (Golden et al., 2019; Manduca et al., 2024; Rava et al., 2025; Schiavi et al., 2022; Schiavi et al., 2023). These phenotypes, together with the well-recognized anatomical and behavioral advantages of rats over mice for modelling neurodevelopmental disorders (Szpirer, 2020; Willemsen and Kooy, 2023), support the use of this animal model to mimic key neurobiological and behavioral deficits that characterize FXS and some of the core and comorbid features of non-syndromic ASD (Golden et al., 2019; Schiavi et al., 2023).

2. Materials and methods

2.1. Animals

Wild-type (WT) (Charles River Laboratories, Italy) and *Fmr1-*$^{\Delta}$*exon 8* male and female rats (Horizon Discovery, formerly SAGE Labs, USA) on Sprague-Dawley background were mated overnight. *Pregnant females* were individually housed in Macrolon cages (40 cm (length) x 26 cm (width) x 20 cm (height)) under controlled conditions (temperature 20–21 °C, 55–65% relative humidity, and 12/12 h light cycle with lights on at 07:00 h).

Newborn litters found before 17:00 h were considered to be born on that day (postnatal day (PND) 0). On PND 1, litters were culled to eight animals (six males and two females) to reduce any litter size-induced variability in the growth and development of pups during the postnatal period. On PND 21, the pups were weaned and housed in groups of three (same sex and genotype). *One male pup per litter, from different litters per group, was randomly selected for each experiment.* All procedures were approved by the Italian Ministry of Health (Rome, Italy) and performed in accordance with the ARRIVE 2.0 (Animals in Research: Reporting In Vivo Experiments) guidelines (Percie du Sert et al., 2020), the guidelines of Italian Ministry of Health (D.L. 26/14; Project authorization n. 65/2023-PR) and the European Community Directive 2010/63/EU.

2.2. Western blotting

Protein expression analysis was performed on samples of WT and *Fmr1-*$^{\Delta}$*exon 8* rats derived from two experimental cohorts. Briefly, rats were sacrificed, their brains were rapidly removed from the skull on a cold plate, and hippocampi were collected and stored at −80 °C until use. Tissue samples were sonicated in ice-cold RIPA buffer supplemented with protease (Cat. 05892791001, Roche) and phosphatase (Cat. 4,906,845,001, Roche) inhibitors, centrifuged at 13,000 xg for 15 min, and supernatants were collected.

Equal amounts of protein (35 μg) from each whole hippocampal lysate was resolved using TGX Stain-Free protein gels under reducing conditions. Subsequently, Stain-Free gel images were acquired using a ChemiDoc XRS + imaging system (Cat.1708265, Bio-Rad) to check sample integrity and separation quality. Gels were electroblotted onto membranes using a Trans-blot Turbo Transfer System (Cat.1704150, Bio-Rad), and a Stain-Free total protein image was acquired to verify protein transfer efficiency and loading control. Then, membranes were blocked in 5% (*w/v*) milk in TBS-T for 60 min at room temperature (RT) and immunoreacted with specific primary antibodies in 2% (w/v) milk in TBS-T at 4 °C overnight (all antibodies used for Western blotting assays are listed in Table 1). After three washes with TBS-T, membranes were incubated with horseradish peroxidase-conjugated secondary antibodies in 2% (w/v) milk in TBS-T for 1 h at RT, washed in TBS, and then developed with chemiluminescence detection reagents (Clarity Western ECL, Cat. 1,705,060, Bio-Rad, USA; WesternBright Sirius HRP substrate, Cat K-12043, Advansta, USA). The chemiluminescent signal was detected by means of the ChemiDoc XRS+ imaging system (Cat. 1,708,265, Bio-Rad) and band intensities were analyzed with Image Lab software. Densitometric values for each sample were normalized to their total protein content. Samples from each cohort were run at least twice on separate gels (technical replicates), and a correction factor was

Table 1
List of antibodies used for Western blotting assays.

Antibody	Dilution	Catalog Number/RRDI	Brand
Anti-GFAP	1:2000	Cat# sc-33,673, RRID: AB_627673	Santa Cruz Biotechnology
Anti-Iba1	1:1000	Cat# A12391, RRID: AB_2759236	ABclonal
Anti-Lamin B1	1:1000	Cat# ab16048, RRID: AB_443298	Abcam
Anti-NF-kB	1:000	Cat# 14–6731-8	Invitrogen
Anti-Caspase 3	1:500	Cat# A19654, RRID: AB_2862718	ABclonal
Anti-Mouse	1:10000	Cat# 7076, RRID: AB_330924	Cell Signaling Technology
Anti-Rabbit	1:3000	Cat# 7074, RRID: AB_2099233	Cell Signaling Technology

applied to adjust for inter-gel variability as previously described (Caffino et al., 2020). Corrected values were then standardized to the mean of the WT group within each cohort to minimize inter-cohort variability. Finally, relative data from both cohorts were pooled into a single dataset for statistical analysis. The abundance of the target protein in *Fmr1-$^{\Delta}$exon 8* rats was expressed as fold change relative to WT controls.

2.3. Proteomic analysis of cytokine expression

The hippocampi of WT and *Fmr1-$^{\Delta}$exon 8* rats were homogenized in PBS (Cat. P4417, Sigma-Aldrich) with protease inhibitors (10 μg/mL Leupeptin, Cat. 1167; 10 μg/mL Aprotinin, Cat. 4139; 10 μg/mL Pepstatin, Cat. 1190, Torcis). After homogenization, Triton X-100 (Cat. X100, Sigma-Aldrich) was added to a final concentration of 1%, and the tissue lysates were centrifuged at 10,000 ×*g* for 5 min to remove cell debris. The protein concentration of the lysates was determined by BCA protein assay (Cat. 23,227, Pierce, Thermo Scientific), and the relative expression of the cytokines was analyzed using the Proteome Profiler Array (Cat. ARY008, Rat Cytokine Array, Panel A; R&D Systems, Minneapolis, MN, USA) according to the manufacturer's protocol with minor modifications (for cytokine array coordinates see Table 2). Briefly, each membrane was incubated for 1 h in 2.0 mL of blocking buffer in a well of a 4-well multi-dish plate on a platform shaker at RT. Parallelly, samples were pooled separately for each experimental group ($n = 5$ WT; n = 5 *Fmr1-$^{\Delta}$exon 8*). Equal amounts of protein (600 μg) from each group were then mixed with the reconstituted detection antibody cocktail and incubated for 1 h at RT. After blocking, membranes were incubated in the sample/antibody solution overnight at 4 °C with agitation. Then, each membrane was washed thrice with 20 mL of 1× Wash Buffer for 10 min and incubated with diluted Streptavidin-HPR (1:2000) for 30 min with agitation at RT. After washing, membranes were incubated with chemiluminescence detection reagent ECL Sirius (Cat. K-12043-D10, Advansta), and the signal was acquired using the ChemiDoc XRS+ imaging system (Cat.1708265, Bio-Rad). Average signals (pixel density) from the pair of duplicate spots representing each cytokine were calculated with the ImageJ/Fiji NIH software (Version 1.51, National Institutes of Health). TIFF pictures were converted to 8-bit and inverted. Each array spot was manually identified using the elliptical ROI (Region of Interest) tool and saved to create an array template. The same set of ROIs was applied identically to all membranes. For each spot, gray values corresponding to each cytokine were averaged and subsequently background-corrected by subtracting the mean intensity of the negative control spots. A comparison of corresponding signals on different arrays to determine the relative change in cytokine levels between groups was performed.

For cytokine expression analysis from peripheral plasma of WT and *Fmr1-$^{\Delta}$exon 8* rats, a Proteome Profiler Array (Cat. ARY008, Rat Cytokine Array, Panel A; R&D Systems, Minneapolis, MN, USA) was also used. Up to 2.5 mL of trunk blood was collected from each animal into 15 mL tubes with EDTA solution (concentration 1:10) (Cat. 15,575–038, Invitrogen, Thermo Fisher Scientific). The tubes were then centrifuged for 20 min at 1000 ×*g* at 4 °C within a maximum of 30 min from collection. Subsequently, the supernatant was collected and stored at −80 °C. Blood sampling procedures were performed according to literature data (Carbone et al., 2023). 200 μl of plasma for each sample were pooled by experimental group ($n = 5$ WT/ n = 5 *Fmr1-$^{\Delta}$exon 8*; 1.0 mL of total volume/group; (Koncekova et al., 2024) and processed according to the manufacturer's protocol.

2.4. Immunofluorescence

Rats were sacrificed, and brains were rapidly removed and fixed in 4% paraformaldehyde (PFA)/PBS solution for immersion for three days. After several washes with PBS, whole brains were cryoprotected in 30% sucrose phosphate buffered solution (PBS, 0.01 M), embedded in the cryo-microtomy embedding medium, frozen in liquid nitrogen, and stored at −80 °C until tissue sectioning. Specimens were cut into 25 μm thick cryostat sections (Leica CM1900 cryostat, Leica Microsystems) in the coronal plane. Sections were wet-mounted on slides, post-fixed in 4% PFA/PBS for 20 min at RT, washed in PBS three times for 5 min each, and permeabilized in PBS-T (PBS supplemented with 0.3% Triton X-100). Sections were then incubated with blocking solution (PBS supplemented with 1% bovine serum albumin (BSA) and 0.3% Triton X-100) for 2 h at RT and immune-stained using primary antibodies anti-Iba1 and anti-GFAP in blocking solution overnight at 4 °C. Subsequently, sections were rinsed in PBS, washed three times for 5 min in PBS-T, and incubated in appropriate secondary conjugated antibodies for 2 h at RT. After washing in PBS-T, nuclei were counterstained with Hoechst 33342 (Thermo Fisher Scientific Inc., Carlsbad, CA). Immunoreaction specificity was assessed by omitting the primary antibodies. All antibodies used in this study for immunofluorescence are listed in Table 3.

For Lamin B1 expression analysis, 5 μm-thicked coronal sections were used, and co-immunofluorescence assays with GFAP were set out. Briefly, brain sections were wet-mounted on slides and dried, then post-fixed in 4% PFA/PBS for 20 min at RT and permeabilized in ice-cold methanol for 10 min. Sections were incubated with blocking solution (PBS supplemented with 5% normal goat serum (NGS) and 5% BSA) for 30 min at RT and immune-stained using primary antibody anti-Lamin B1 in blocking solution overnight at 4 °C. Subsequently, sections were rinsed in PBS, washed three times for 5 min in PBS-T (0.1% Triton X-100) and incubated in the goat anti-Rabbit IgG Secondary Antibody, Alexa Fluor™ 488 in PBS for 1 h at RT. After washing in PBS-T, sections were incubated with the primary anti-GFAP in 1% BSA/PBS overnight at 4 °C, then rinsed in PBS, washed three times for 5 min in PBS-T, and

Table 2
Rat cytokine array coordinates (Adapted from Cat. ARY008, Rat Cytokine Array, Panel A; R&D Systems).

Rat Cytokine Array Panel A Coordinates										
Spots	1_2	3_4	5_6	7_8	9_10	11_12	13_14	15_16	17_18	19_20
a	Reference	CINC-1	CINC-2α/β	CINC-3	CTNF	CX3CL1	GM-CSF	ICAM-1	IFN-γ	Reference
b	/	IL-1α	IL-1β	IL-1rα	IL-2	IL-3	IL-4	IL-6	IL-10	/
c	/	IL-13	IL-17	IP-10	LIX	L-Selectin	MIG	MIP-1α	MIP-3α	/
d	Reference	RANTES	CXCL7	TIMP-1	TNF-α	VEGF	/	/	CTRL (−)	/

Table 3
List of antibodies used for immunostaining.

Antibody	Dilution	Catalog Number	Brand
Mouse Anti-GFAP	1:50	Cat# sc-33,673, RRID: AB_627673	Santa Cruz Biotechnology
Rabbit Anti-Iba1	1:1000	Cat# 019–19,741, RRID: AB_839504	FUJIFILM Wako Pure Chemical Corporation
Rabbit Anti-Lamin B1	1:500	Cat# ab16048, RRID: AB_443298	Abcam
Goat Anti-Mouse Alexa 555	1:500	Cat # A-21422	Thermo Fisher Scientific
Goat Anti-Rabbit Alexa 488	1:500	Cat # A-11008	Thermo Fisher Scientific

finally incubated in goat anti-Mouse IgG Secondary Antibody, Alexa Fluor™ 555 in PBS for 1 h at RT. Nuclei were counterstained with Hoechst 33342 (Thermo Fisher Scientific Inc., Carlsbad, CA). Immunoreaction specificity was assessed by omitting the primary antibodies.

2.5. Image acquisition and analysis

Immunostained brain samples were firstly acquired at a digital slide scanner platform (Nanozoomer S60, Hamamatsu, Shizuoka, Japan) allowing to obtain whole tissue slice images by Tile Scan function. They were acquired at a Leica TCS-SP8X confocal microscope (Leica Microsystems, Mannheim, Germany) using 20×/dry, 40×/oil or 63×/oil immersion objectives and the LAS X software. The number of Iba1-positive and GFAP-positive cells was determined in fixed ROIs of 500 μm^2 in the CA1 and DG regions of the hippocampus for each animal ($n = 4$ WT/ n = 4 *Fmr1-$^{\Delta}$exon 8*). Cells were manually counted on acquired images at 20× magnification by using the Cell Counter plugin from the ImageJ/Fiji NIH software (Version 1.51, National Institutes of Health).

In addition, individual Iba1-positive microglia and GFAP-positive astrocytes (n = 12 cells/1–3 ROI/ 4 rats) were selected in the hippocampal CA1 and DG subregions and analyzed for morphometric parameters describing the cell shape and spatial structure by ImageJ/Fiji NIH software as previously described (Young and Morrison, 2018). Cell inclusion was based exclusively on predefined technical inclusion criteria. Only cells entirely contained in the image with full visualization of cell morphology across all processes and the absence of overlapping cells or tissue artifacts, were included in the analysis. Morphometric analyses were independently performed for each hippocampal subregions and no direct comparisons were conducted between CA1 and DG.

Briefly, fluorescent images were converted into representative binary images and analyzed by using ImageJ/Fiji NIH software plugins Analyze Skeleton and FracLac for morphology data collection. Total branches, average length, endpoints, and junction number were calculated from the skeletonized image.

The same cells were also assessed with the FracLac plugin to determine fractal dimension, lacunarity, span ratio, and density as complexity cell shape and size descriptors (Green et al., 2022; Young and Morrison, 2018). In addition, for each Iba1-positive microglia, the soma perimeter, area and arborization domain were computed. In particular, soma area and perimeter were determined by drawing a line around the cell body by using the ImageJ freehand selection tool. The extent of microglia ramification was quantified by measuring the area circumscribed by the distal ends of each process using the polygon selection tool (arborization area) (Basilico et al., 2019). A morphological index was also determined using the formula: soma area/arborization area. The larger the value, the greater the soma size was related to the arbor size (Tremblay et al., 2012). The mean fluorescence intensity (MFI) of Lamin B1 and nuclear dysmorphisms were analyzed in confocal images acquired using 63× magnification by ImageJ/Fiji NIH software.

2.6. Statistical analysis

Statistical analyses were performed with GraphPad Prism 8.0 software.

Data distribution was assessed using the Shapiro-Wilk test and Q-Q plots. Parametric *t*-tests (t-test with Welch's correction) were applied only when normality assumptions were satisfied; if the Shapiro–Wilk test rejected the null hypothesis of normality, a nonparametric test (i.e., Mann-Whitney test) was applied. Potential outliers within each dataset were identified using GraphPad Prism version 8.0 (Grubbs' method); this method was not applied as an automatic criterion for data exclusion. The number of animals used for this study was as follows: $n = 4$ WT and n = 4 *Fmr1-$^{\Delta}$exon 8* rats for immunofluorescence assays, $n = 8$ WT and n = 8–9 *Fmr1-$^{\Delta}$exon 8* rats for western blot experiments, $n = 5$ WT and n = 5 *Fmr1-$^{\Delta}$exon 8* rats for cytokine expression analysis. Data are presented as mean ± standard deviation (SD), with each dot representing an individual animal. Statistical details (test used, sample size, *p*-value) can be found in figure legends and in Supplementary Tables 1–5.

3. Results

3.1. Altered microglia density and morphology in the hippocampus of young adult *Fmr1-$^{\Delta}$exon 8* rats

Microglia are highly dynamic resident immune cells that play key roles in brain development, maintenance, and neuroimmunity (Colonna and Butovsky, 2017). Given their pronounced sensitivity to local tissue dyshomeostasis, microglia can undergo morpho-functional, proliferative, and biochemical adaptations in response to even subtle changes in the brain parenchyma (Wang et al., 2025).

Since several neuropathological changes were described both in individuals with FXS and *Fmr1* KO mice (Bagni and Zukin, 2019; Y. S. Chen et al., 2022a), we first examined whether young adult male *Fmr1-$^{\Delta}$exon 8* rats showed alterations in the local density of microglia by immunostaining for the Ionized calcium-binding adapter molecule 1 (Iba1) marker, a cytoskeletal protein specific for microglia and macrophages and commonly used in histological evaluation (Ito et al., 1998). We focused our attention on the hippocampus (Fig. 1a, b), a brain region related to memory formation and consolidation and found to be significantly affected in FXS (Bhandari et al., 2024; Bostrom et al., 2016; Tian et al., 2017). Interestingly, we found a significant increase in the number of Iba1-positive microglia in the CA1 subfield of the hippocampus of *Fmr1-$^{\Delta}$exon 8* rats compared to age-matched WT control rats (Fig. 1c), while no evident alterations of microglial density were observed in the DG (Fig. 1d), which may reflect distinct neuronal and synaptic microenvironments between these hippocampal subfields (Alkadhi, 2019). This could suggest an increased vulnerability of the hippocampal CA1 subfield in FXS, in line with the key role played by this hippocampal subregion in the cognitive deficits displayed by models of FXS (Kalinowska et al., 2022; Manduca et al., 2024; Rava et al., 2025; Sawicka et al., 2019; Schiavi et al., 2023).

We next decided to assess the morphological profile of mutant CA1 and DG microglial cells. Quantitative analysis of microglial morphology in *Fmr1-$^{\Delta}$exon 8* rats revealed that Iba1-positive CA1 microglia are characterized by a reduced number of branches, junctions and end-point voxels in adult *Fmr1-$^{\Delta}$exon 8* rats compared to age-matched WT (Fig. 1e, f). Furthermore, although density, span ratio, and lacunarity resulted similar between genotypes, the fractal dimension parameter was significantly decreased in *Fmr1-$^{\Delta}$exon 8* rats. CA1 microglia also exhibited larger soma area, smaller arborization, and higher morphological index compared to WT rats (Supplementary Fig. 1, CA1). Microglial arborization was similarly affected in the DG of the hippocampus in *Fmr1-$^{\Delta}$exon 8* rats (Fig. 1g, h). In this region, no significant changes in soma size of microglial cells were observed; however, the morphological index was increased due to a reduction in arborization area (Supplementary Fig. 1, DG). As Iba1 expression is thought to

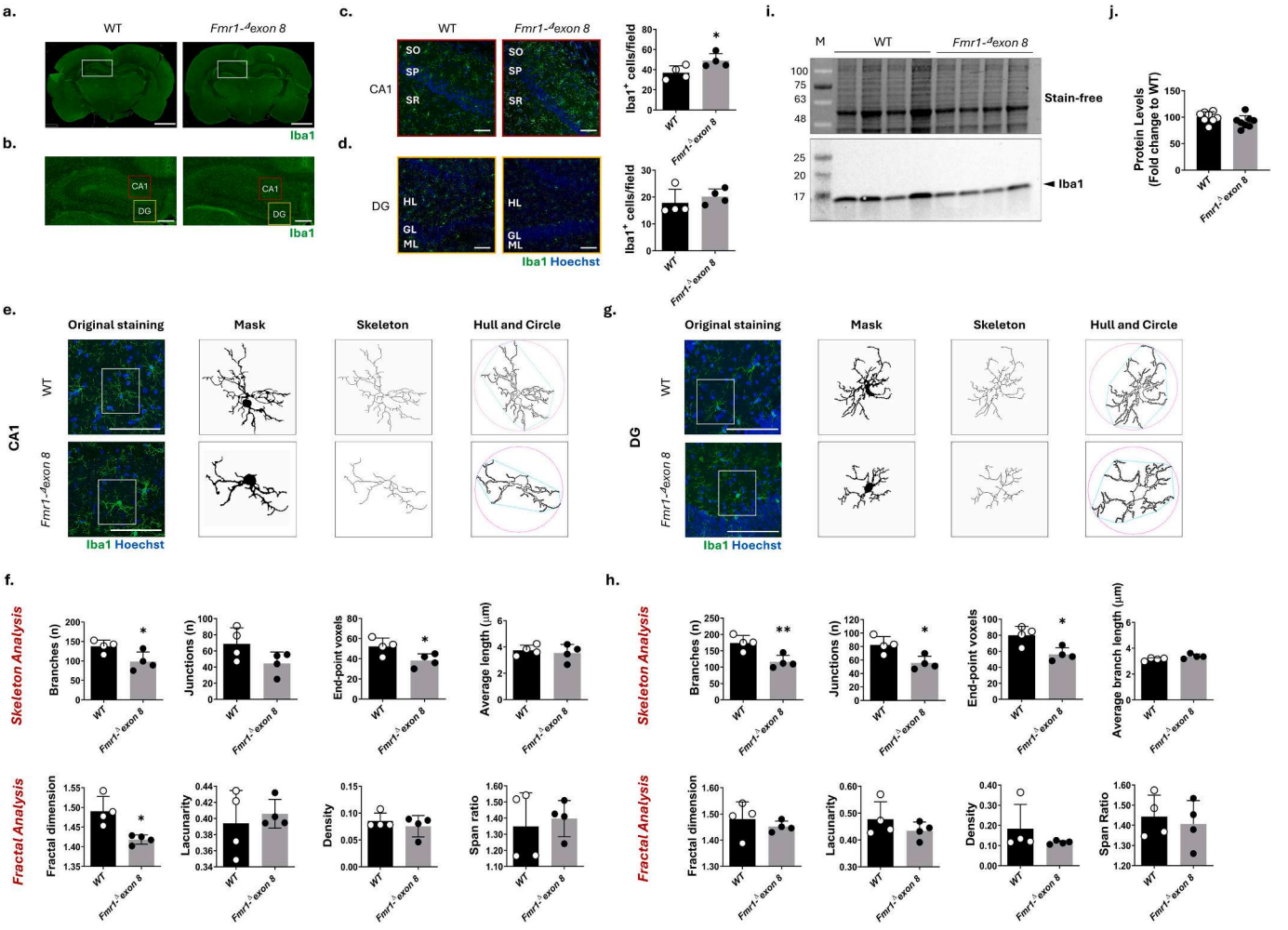

Fig. 1. Altered Iba1-positive microglial density and morphology in the hippocampus of *Fmr1-*$^{\Delta}$*exon 8* rats.
(a) Representative digital scanner images of whole-brain sections from adult WT and *Fmr1-*$^{\Delta}$*exon 8* rats stained with the Iba1 microglial marker. Scale bars, 2.5 mm. Hippocampal regions are highlighted by white insets and enlarged in (b). (b) Representative images of the hippocampal region of adult WT and *Fmr1-*$^{\Delta}$*exon 8* rats stained for Iba1. Scale bars, 500 µm. The CA1 subfield (highlighted with red inset) and the DG (highlighted with yellow inset) analyzed for microglial density are enlarged respectively in (c) and (d). (c, d) Representative confocal microscopy images (left panels) and quantitative analysis (right panels) of Iba1-positive microglia cells in the CA1 (in (c) – red-highlighted panels) and in the DG (in (d) - yellow-highlighted panels) of WT and *Fmr1-*$^{\Delta}$*exon 8* rats at PND 75. Quantification was performed by counting Iba1-positive microglia per field (500 µm^2). Scale bars, 100 µm. Data are presented as mean ± SD (Welch's t-test and Mann-Whitney test, *p < 0.05; $n = 4$ WT/ n = 4 *Fmr1-*$^{\Delta}$*exon 8*). (e, g) Confocal photomicrographs of Iba1-stained microglia (left panel) with corresponding binary, skeletonized and outline images (right panels) from the CA1 (e) and DG (g) subfields of WT and *Fmr1-*$^{\Delta}$*exon 8* rats. Scale bar, 100 µm. (f, h) Skeleton and fractal analyses of microglia from hippocampal CA1 (f) and DG (h) subfields of WT and *Fmr1-*$^{\Delta}$*exon 8* rats. Data are presented as mean ± SD (Welch's t-test and Mann-Whitney test, *p < 0.05,**p < 0.01; n = 4 WT/ n = 4 *Fmr1-*$^{\Delta}$*exon* 8 rats). (i, j) Representative western blot (i) and relative quantification (j) of Iba-1 protein expression in total hippocampal lysates from adult male WT and *Fmr1-*$^{\Delta}$*exon 8* rats (black filled bars: WT rats; gray filled bars: *Fmr1-*$^{\Delta}$*exon 8* rats). Densitometric values were normalized to the total protein content visualized by using Stain-Free technology. Data from two independent cohorts are presented as mean ± SD (Welch's t-test, $n = 8$ WT (black filled bars)/ 8 *Fmr1-*$^{\Delta}$*exon 8* (gray filled bars)). Original blots are shown in Supplementary Fig. 2. Additional statistical details are provided in Supplementary Table 1. Abbreviations: M, protein marker, HL, hilus, CA1, cornu ammonis 1; DG, dentate gyrus, GL, granular layer, ML, molecular layer, SO, stratum oriens, SP, stratum pyramidale, SR, stratum radiatum. (For interpretation of the references to colour in this figure legend, the reader is referred to the web version of this article.)

increase under some pathological and experimental conditions (Lier et al., 2021), we also performed Western blotting experiments to analyze its relative protein expression in total hippocampal lysates from adult male *Fmr1-*$^{\Delta}$*exon 8* rats. We did not find significant changes in Iba1 protein expression in the hippocampus of adult male *Fmr1-*$^{\Delta}$*exon 8* rats compared to age-matched WT controls (Fig. 1i, j). Consistently, previous works also failed to reveal a significant induction of Iba1 expression (Blandin et al., 2024; Hodges et al., 2020; Pacey et al., 2015) in several brain areas, such as the cortex (Lee et al., 2019), hippocampus (Blandin et al., 2024), cerebellum (Pacey et al., 2015) and auditory brainstem nuclei (Rotschafer and Cramer, 2017) in adult *Fmr1* KO mice under steady-state conditions. Taken together, these findings indicate a less complex cellular architecture in *Fmr1-*$^{\Delta}$*exon 8* rats compared with WT microglia, although its functional significance remains to be further investigated.

3.2. *No evidence of an overt cytokine-mediated pro-inflammatory response in the hippocampus of young adult Fmr1-*$^{\Delta}$*exon 8 rats*

Although previous studies have shown an increased brain and peripheral innate immune activation in individuals suffering from ASD and in preclinical ASD models, often associated with behavioral impairments (Hughes et al., 2023), inflammatory processes have not been extensively studied in FXS. Here, we analyzed the expression levels of 19 inflammatory mediators in brain and plasma of *Fmr1-*$^{\Delta}$*exon 8* rats compared to WT controls. We did not observe a marked upregulation of specific

cytokines/chemokines neither in plasma samples nor in hippocampal lysates from *Fmr1-Δexon 8* rats (Fig. 2a-f). In the hippocampus, a subset of inflammatory mediators exhibited modest expression changes, whereas others remained unchanged (Fig. 2a-c). Specifically, CX3CL1 (*C*-X3-C motif chemokine ligand 1), and CNTF (Ciliary Neurotrophic Factor) were reduced in *Fmr1-Δexon 8* rats, while ICAM-1 (Intercellular Adhesion Molecule-1), CXCL7 (C-X-C motif chemokine ligand 7), VEGF (Vascular Endothelial Growth Factor), and LIX (Lipopolysaccharide-Induced CXC Chemokine) were detectable but did not display genotype-dependent differences. In the plasma, IL1α (Interleukin 1 alpha) and CINC-1 (Cytokine-Induced Neutrophil Chemoattractant-1) were slightly reduced compared to controls (Fig. 2d-f). Consistent with the absence of robust genotype-dependent differences in cytokine profiles between WT and *Fmr1-Δexon 8* rats under the conditions tested, we also failed to detect a significant upregulation of protein levels of Nuclear factor-κB (NF-κB), a master regulator of the immune response, in the hippocampus of mutant animals (Fig. 2g, h). Collectively, these findings indicate that the local alterations in hippocampal glial cell morphology and density occur in the absence of detectable evidence for a cytokine-mediated inflammatory response in the *Fmr1-Δexon 8* rat model under the experimental conditions examined.

3.3. Altered astrocyte density and morphology in the hippocampus of young adult *Fmr1-Δexon 8* rats

Microglia can modify neuronal structure and activity via crosstalk with astrocytes, which also express FMRP (Pacey and Doering, 2007) and have been involved in the pathogenesis of FXS. Indeed, multiple astrocytic alterations have been described in FXS (D'Antoni et al., 2024).

In the present study, we assessed the astrocyte profile in the hippocampus of young adult male *Fmr1-Δexon 8* rats by investigating the local density, the relative GFAP expression and the astrocyte morphology. Immunofluorescence analysis revealed a significant increment of the GFAP-positive cell number both in the CA1 (Fig. 3c) and DG (Fig. 3d) subfields of the hippocampus of *Fmr1-Δexon 8* rats compared to controls.

However, Western blotting analysis did not show a significant increase in GFAP protein expression in total hippocampal lysates from male *Fmr1-Δexon 8* rats (Fig. 3e, f). We then performed a comparative morphometric investigation of hippocampal astrocytes in the CA1 (Fig. 3g, h) and DG (Fig. 3i, j) subfields. We failed to find hypertrophic astrocytes, often associated with a reactive phenotype. However, we found that astrocytes of *Fmr1-Δexon 8* rats showed a markedly reduced number of branches, junctions and end-points along with a decreased fractal dimension parameter in these two brain regions. These morphological changes indicate that astrocytes in *Fmr1-Δexon 8* rats are less complex and ramified compared to WT control rats.

3.4. Reduced level of Lamin B1 and dysmorphic nuclei in the hippocampus of *Fmr1-Δexon 8* rats

In the rodent brain, Lamin B1 can be detected in both neuronal and glial cells (Takamori et al., 2018), and it is involved in multiple key cell functions (Sobo et al., 2024). Previous reports showed that Lamin B1 deregulations can severely impact astroglia activation, neuronal activity and neuro-gliogenesis leading to behavioral abnormalities (Bedrosian et al., 2021; Ratti et al., 2021). Moreover, a decline in Lamin B1 expression and defective nuclear morphology have been found to be cell hallmarks of aging and several neurodegenerative disorders, primarily affecting astrocytes (Koufi et al., 2023). On this basis, we examined the levels of Lamin B1 expression in the hippocampal CA1 and DG subfields of adult WT and *Fmr1-Δexon 8* rats by immunofluorescence analysis (Fig. 4a). Quantification of immunostaining revealed an overall reduction in the Mean Fluorescence Intensity (MFI) of Lamin B1 in the stratum radiatum, stratum pyramidale, and stratum oriens of the CA1 subfield as well as in the DG in *Fmr1-Δexon 8* rats compared to WT controls (Fig. 4b). In line with these results, reduced Lamin B1 protein expression was also

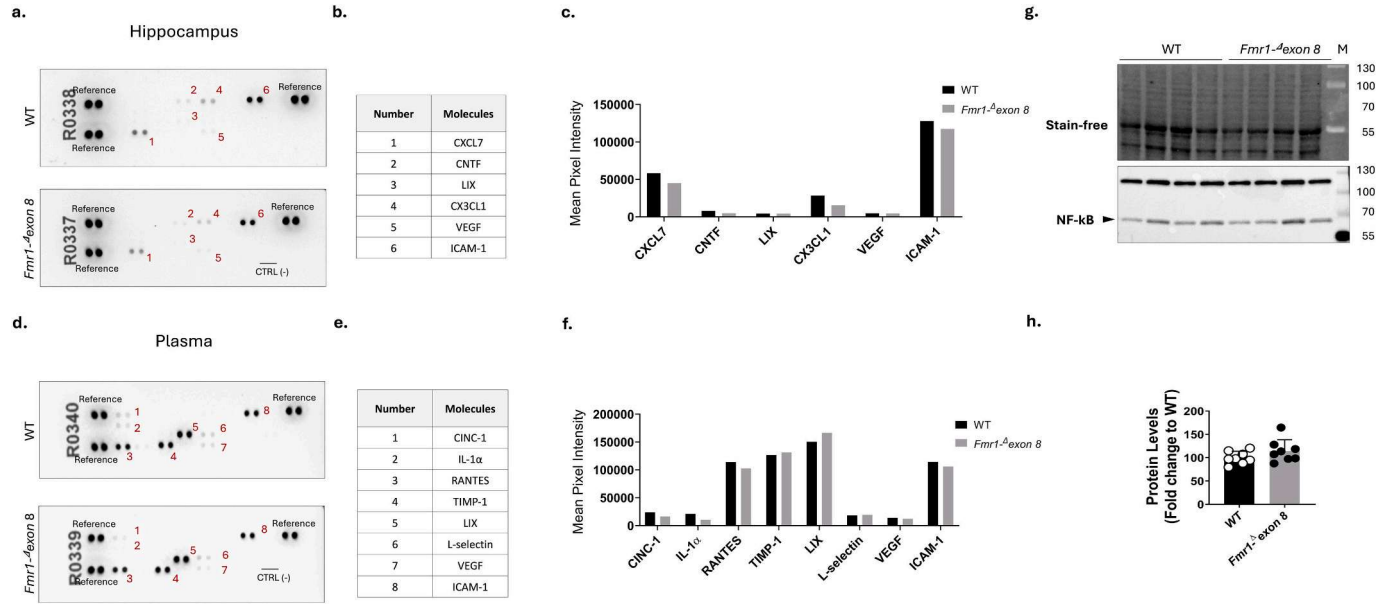

Fig. 2. No evidence of an overt cytokine-mediated pro-inflammatory profile in *Fmr1-Δexon 8* rats.
(a, d) Cytokine proteome profiler array from total hippocampal lysates (a) and plasma (d) of young adult WT and *Fmr1-Δexon 8* rats at PND 75 ($n = 5$ rats per group, 600 μg from five pooled hippocampi per group or 1 mL from five pooled plasma per group were run on each array). Cytokines detected in the hippocampus and plasma of WT and *Fmr1-Δexon 8* rats are identified by numerical labels and listed in the relative Table (b, e). Spatial coordinates of each cytokine on the arrays are provided in Table 2. (c, f) The array data were quantitated to generate a proteome profile (histogram). Array images were collected using the ChemiDoc XRS+ imaging system and analyzed by ImageJ/Fiji NIH software.
(g, h) Representative western blot (g) and relative quantification (h) of NF-κB protein expression in total hippocampal lysates from adult male WT and *Fmr1-Δexon 8* rats are shown. Densitometric values were normalized to the total protein content visualized by using Stain-Free technology. Data from two experimental cohorts are presented as mean ± SD (Welch's t-test, n = 8 WT (black filled bars)/ n = 8 *Fmr1-Δexon 8* rats (gray filled bars)). Additional statistical details are provided in Supplementary Table 2. Original blots are shown in the Supplementary Fig. 3. Abbreviations: M, protein marker.

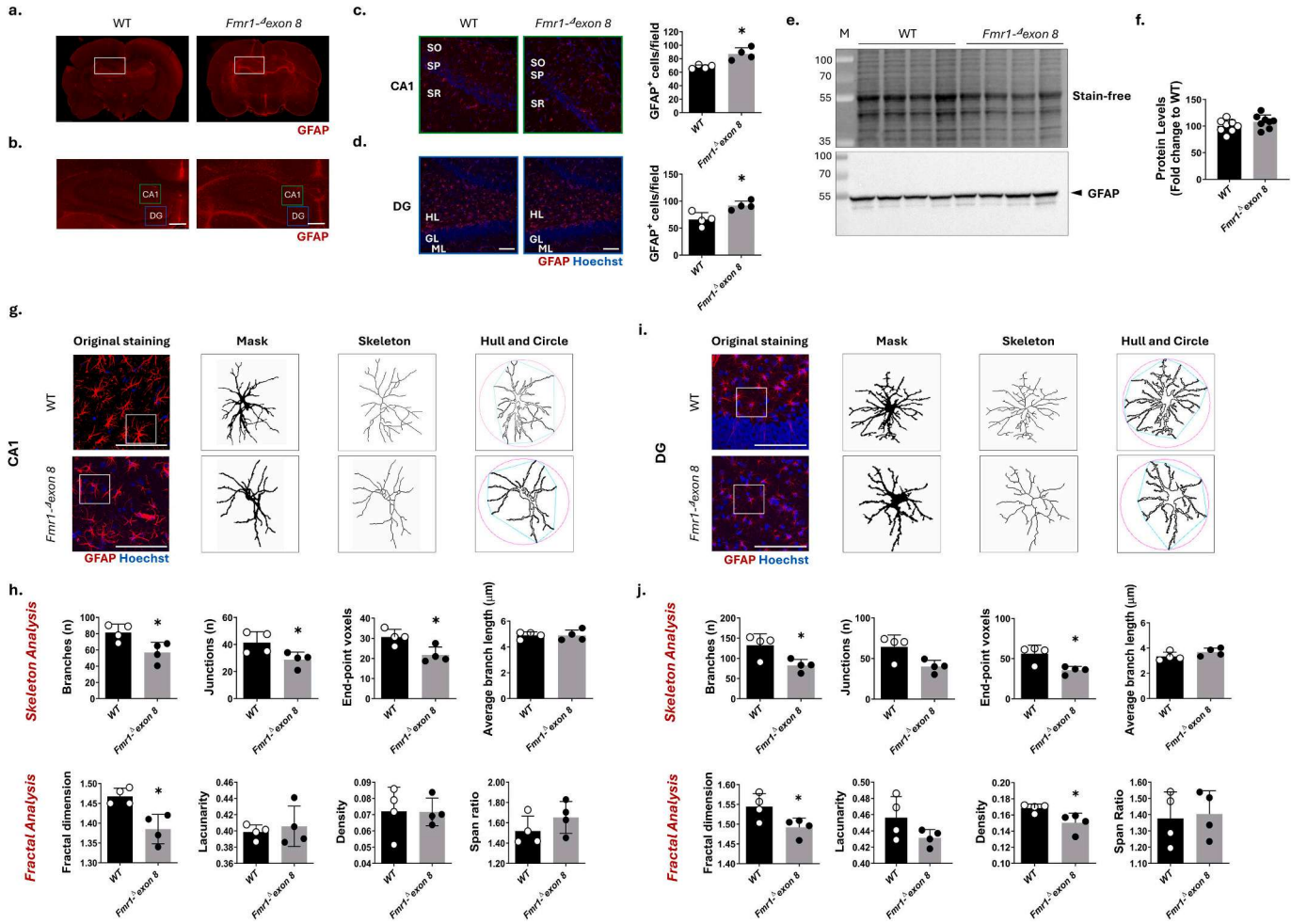

Fig. 3. Altered density and morphology of GFAP-positive astrocytes in the hippocampus of *Fmr1-Δexon 8* rats.
(a) Representative digital scanner images of whole-brain sections of adult WT and *Fmr1-Δexon 8* rats stained for GFAP marker. Scale bars, 2.5 mm. Hippocampal regions are highlighted by white inserts and enlarged in (b). (b) Representative images of the hippocampal region of adult WT and *Fmr1-Δexon 8* rats stained for the GFAP marker. Scale bars, 500 µm. The CA1 subfield (highlighted with green inset) and the DG (highlighted with blue inset) are enlarged respectively in (c) and (d). (c, d) Representative confocal microscopy images (left panels) and quantitative analysis (right panels) of GFAP-positive astrocyte in the CA1 (in (c) – green-highlighted panels) and DG (in (d) - blue-highlighted panels) of adult WT and *Fmr1-Δexon 8* rats. Quantification was performed by counting GFAP-positive astrocyte per ROI (500 µm^2). Scale bars, 100 µm. Data are presented as mean ± SD (Welch's t-test, *$p < 0.05$; n = 4 WT (black bars)/ n = 4 *Fmr1-Δexon 8* (gray bars)). (e, f) Representative western blot (e) and relative quantification (f) of GFAP protein expression in total hippocampal lysates from adult male WT and *Fmr1-Δexon 8* rats (black filled bars: WT rats; gray filled bars: *Fmr1-Δexon 8* rats). Densitometric values were normalized to the total protein content visualized by using Stain-Free technology. Data from two independent cohorts are presented as mean ± SD (Welch's t-test, n = 8 WT (black filled bars)/ 8 *Fmr1-Δexon 8* (gray filled bars)). Original blots are shown in the Supplementary Fig. 4. (g, i) Confocal photomicrographs of GFAP-stained astrocytes (left panel) with corresponding binary, skeletonized and outline images (right panels) from the CA1 (g) and DG (i) subfields of WT and *Fmr1-Δexon 8* rats. Scale bar, 100 µm. (h, j) Skeleton and fractal analyses of GFAP-stained astrocytes from hippocampal CA1 (h) and DG (j) subfields of WT and *Fmr1-Δexon 8* rats. Data are presented as mean ± SD (Welch's t-test and Mann-Whitney test, *$p < 0.05$; n = 4 WT/ n = 4 *Fmr1-Δexon* 8 rats). Additional statistical details are provided in Supplementary Table 3.
Abbreviations: M, protein marker, HL, hilus, CA1, cornu ammonis 1; DG, dentate gyrus, GL, granular layer, ML, molecular layer, SO, stratum oriens, SP, stratum pyramidale, SR, stratum radiatum. (For interpretation of the references to colour in this figure legend, the reader is referred to the web version of this article.)

reported in total hippocampal lysates of *Fmr1-Δexon 8* rats (Fig. 4c, d). Subsequently, since Lamin B1 content is essential in regulating nuclear lamina assembly and therefore in maintaining structural and functional integrity of the nucleus (Kim, 2023), we investigated the number of dysmorphic nuclei in the hippocampal CA1 and DG subregions. A significant increase in the percentage of cells with nuclear deformations was found in both hippocampal regions in *Fmr1-Δexon 8* rats compared to controls, suggesting a positive correlation between Lamin B1 intensity decline and the occurrence of nuclear abnormalities in *Fmr1-Δexon 8* rats (Fig. 4e, f). Given that an intact lamina has been shown to delay the execution of programmed cell death (Lindenboim et al., 2020), a Lamin B1 deficiency in the hippocampus of *Fmr1-Δexon 8* rats might correlate with increased levels of apoptosis. To test this possibility, we also analyzed the relative protein expression of caspase-3, a key enzyme in programmed cell death. Contrary to our expectations, we observed a marked reduction in caspase-3 in *Fmr1-Δexon 8* rats (Supplementary Figs. 6 and 7).

3.5. Hippocampal glia shows nuclear alterations and reduced levels of Lamin B1 in Fmr1-Δexon 8 rats

Given the density and morphological changes found in hippocampal astrocytes and microglia of *Fmr1-Δexon 8* rats as well as the alterations in the Lamin B1 reported in the same region of the hippocampus, we then investigated whether these glial cells showed Lamin B1 loss and nuclear abnormalities. We found that the GFAP-positive astrocytes in the CA1 subfield displayed a significant reduction of Lamin B1 expression, as evaluated by MFI analysis, as well as alterations in the nuclear size and

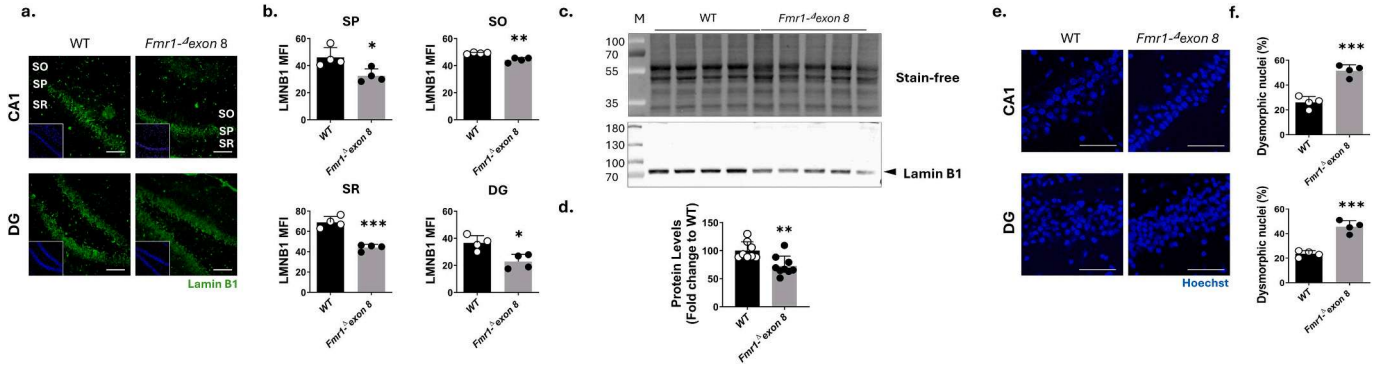

Fig. 4. Reduced levels of Lamin B1 and dysmorphic nuclei in the hippocampus of *Fmr1-$^{\Delta}$exon 8* rats.
(a, b) Representative confocal microscopy images (a) and quantitative analysis (b) of MFI of Lamin B1 in the hippocampal CA1 subfield layers (stratum pyramidale, stratum oriens, and stratum radiatum) and in the DG of WT and *Fmr1-$^{\Delta}$exon 8* rats at PND 75. Scale bars, 100 μm. Data are presented as mean ± SD (Welch's t-test, *p < 0.05, **p < 0.01, ***p < 0.001; n = 4 WT (black bars)/ n = 4 *Fmr1-$^{\Delta}$exon 8* rats (gray bars)).
(c, d) Representative western blot (c) and relative quantification (d) of Lamin B1 protein expression in total hippocampal lysates from adult male WT and *Fmr1-$^{\Delta}$exon 8* rats. Densitometric values were normalized to the total protein content visualized using Stain-Free technology. Data from two experimental cohorts are presented as mean ± SD (Mann-Whitney test, **p < 0.01; n = 8 WT (black filled bars)/ *n* = 9 *Fmr1-$^{\Delta}$exon 8* (gray filled bars)). Original blots are shown in the Supplementary Fig. 5. (e, f) Representative high magnification confocal images (e) and quantification of the percentage of dysmorphic nuclei (f) in the hippocampal CA1 pyramidal layer and hippocampal DG granule cell layer of WT and *Fmr1-$^{\Delta}$exon 8* rats at PND 75. Scale bars, 50 μm. Data are presented as mean ± SD (Welch's t-test, ***p < 0.001; n = 4 WT (black filled bars)/ n = 4 *Fmr1-$^{\Delta}$exon 8* rats (gray filled bars)). Additional statistical details are provided in Supplementary Table 4.
Abbreviations: M, protein marker; LMNB1, Lamin B1, MFI, Mean Fluorescent Intensity, CA1, cornu ammonis 1; DG, dentate gyrus, SO, stratum oriens, SP, stratum pyramidale, SR, stratum radiatum.

shape (Fig. 5a-c). Indeed, area, minor axis and perimeter along with morphometric parameters related to nuclear shape irregularity, such as circularity and roundness, were significantly decreased (Fig. 5c). Similar to astrocytes, microglia displayed altered nuclear morphological descriptors (Fig. 5d, e), suggesting that defective nuclear morphology might be an early hallmark of glia cells in the FXS.

4. Discussion

A growing body of evidence suggests that glial cells contribute to the pathophysiology of FXS, a neurodevelopmental disorder characterized by the loss of the RNA-binding protein FMRP (Hughes et al., 2023). FMRP is expressed in both astrocytes and microglia during postnatal brain development. Although its levels decline over time in a region-specific manner, FMRP remains present in the mature brain (D'Antoni et al., 2024; Gholizadeh et al., 2015; Pacey and Doering, 2007). Consequently, developmental and adult FMRP deficiency results in several biochemical and functional changes in glial cells (Talvio and Castren, 2023), potentially increasing susceptibility to ASD and FXS-like phenotypes (J. L. Hodges et al., 2017b; Hooshmandi et al., 2025).

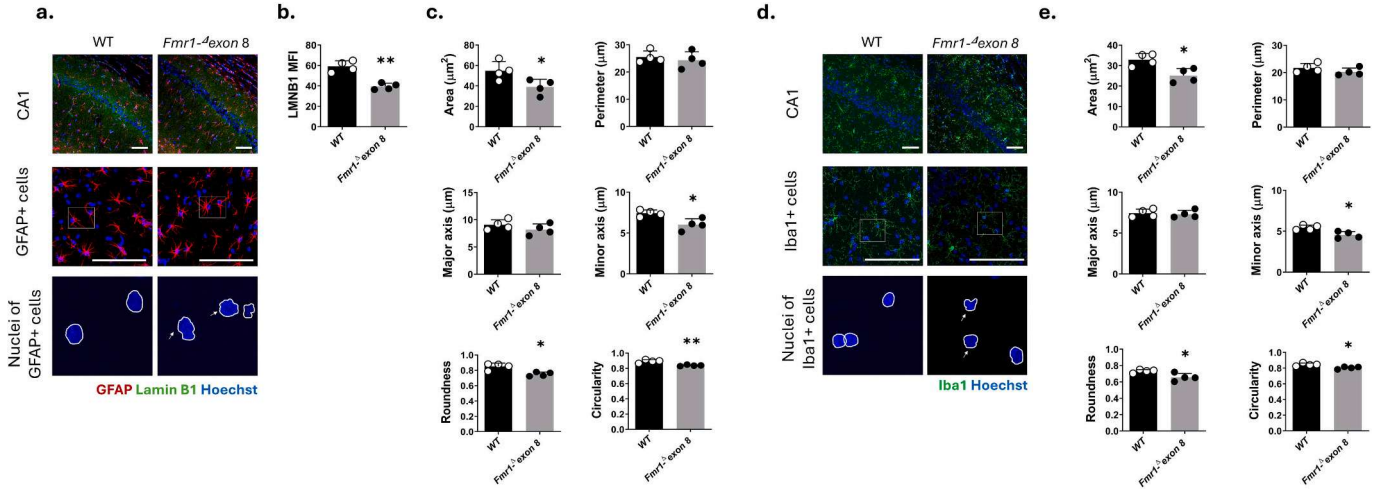

Fig. 5. Hippocampal astrocytes and microglia show nuclear alterations and reduced levels of Lamin B1 in *Fmr1-$^{\Delta}$exon 8* rats.
(a) Representative confocal images of GFAP-positive astrocytes and Lamin B1 staining in the hippocampal CA1 subfield (upper panels). Lower panels show a higher magnification of GFAP-positive astrocytes (in the middle) and some selected Hoechst-stained nuclei (in the bottom), with altered nuclear morphology (highlighted with white outline and white arrows) in CA1 astrocytes in *Fmr1-$^{\Delta}$exon 8* rats. (b, c) Quantitative analysis of MFI of Lamin B1 (b) and nuclear shape descriptors (c) in astrocytes of the hippocampal CA1 subfield of WT and *Fmr1-$^{\Delta}$exon 8* rats at PND 75 (MFI analysis: Welch's t-test, **p < 0.01. Morphometric analysis: Welch's t-test, *p < 0.05, **p < 0.01; n = 4 WT (black filled bars)/ n = 4 *Fmr1-$^{\Delta}$exon 8* (gray filled bars)). (d) Representative confocal images of Iba1-positive microglia in the hippocampal CA1 subfield (upper panels). Lower panels show a higher magnification of Iba1-positive microglia (in the middle) and some selected Hoechst-stained nuclei (in the bottom), showing altered nuclear morphology (highlighted with white outline and white arrows) in CA1 microglia in *Fmr1-$^{\Delta}$exon 8* rats. (e) Quantitative analysis of nuclear shape descriptors in the hippocampal CA1 microglia of WT and *Fmr1-$^{\Delta}$exon 8* rats at PND 75. Scale bars, 100 μm. Data are presented as mean ± SD (Welch's t-test, *p < 0.05; n = 4 WT (black filled bars)/ n = 4 *Fmr1-$^{\Delta}$exon 8* (gray filled bars)). Additional statistical details are provided in Supplementary Table 5. Abbreviations: MFI, Mean Fluorescent Intensity, CA1, cornu ammonis 1.

In the present study, we found that the *Fmr1-*$^{\Delta}$*exon 8* rat model of FXS displays both structural and numerical changes in microglial cells and astrocytes within the hippocampus, without evidence of significant induction of pro-inflammatory cytokines. Indeed, we observed a region-specific increase in the number of Iba1-positive microglial cells in the CA1 subfield of *Fmr1-*$^{\Delta}$*exon 8* rats compared to WT controls, while no significant changes were detected in the DG. Moreover, microglia cells in these regions displayed enlarged soma and less ramified, less complex morphology (though not amoeboid), features previously associated to reactive-phenotypes (Lee et al., 2017). Nevertheless, we explicitly acknowledge that morphological alterations alone are insufficient to infer specific functional states or to discriminate between homeostatic and disease-associated conditions (Lier et al., 2021; Paolicelli et al., 2022).

To determine whether the morphological changes observed in microglia reflect an inflammatory response, we analyzed cytokines and chemokines expression in the plasma and hippocampus of *Fmr1-*$^{\Delta}$*exon 8* rats, along with the protein levels of NF-κB - an inducible transcription factor that regulates several genes involved in inflammatory responses (Liu et al., 2017). Under the experimental conditions tested, we did not detect a substantial upregulation of specific inflammatory cytokine or chemokines in *Fmr1-*$^{\Delta}$*exon 8* rats compared to controls. Similarly, NF-κB protein levels did not differ significantly between genotypes, further supporting the notion that overt inflammation might not be an early hallmark of FXS. It should be noted that membrane-based cytokine immunoassays yield semi-quantitative data, and sample pooling limits sensitivity to subtle, heterogeneous, or subgroup-specific effects, while precluding formal statistical testing. Accordingly, the present findings should be interpreted within this methodological context, and further validation using individual samples will be important to strengthen and extend these observations. Nevertheless, our results are consistent with previous studies reporting no compelling evidence for sustained pro-inflammatory cytokine expression in the hippocampus (S. L. Hodges et al., 2017a; Hodges et al., 2020; Pietropaolo et al., 2014; Santana-Coelho and Lugo, 2023) or serum of FXS mouse models (Yuskaitis et al., 2010) and in individuals with FXS (Ashwood et al., 2011; Van Dijck et al., 2020), despite reports of an increased incidence of infectious conditions in this population (Yu et al., 2020). This contrasts with findings in ASD, a condition frequently comorbid with FXS, where inflammatory processes appear to be more prominent (Hughes et al., 2023; Siniscalco et al., 2018).

Prior studies have shown that *Fmr1*-deficient mice exhibit exaggerated upregulation of complement components and inflammatory mediators in response to immune-activating lipopolysaccharide (LPS) exposure (Hodges et al., 2020; Santana-Coelho and Lugo, 2023). Likewise, *Fmr1*-deficient microglia showed increased inflammatory and phagocytic response following LPS stimulation in vitro (Parrott et al., 2021), further supporting the view that inflammatory alterations in FXS are context- and stimulus-dependent rather than indicative of chronic basal inflammation. Importantly, given the well-documented variability in immune responses across rodent strains and the even greater differences between rodents and humans (Mestas and Hughes, 2004; Zschaler et al., 2014), findings related to immune function and inflammation should be interpreted with caution from a translational perspective. Rodent models may not fully recapitulate the temporal, cellular, and molecular heterogeneity observed in individuals with FXS.

Fmr1 is broadly expressed throughout the brain, including the hippocampus, during early postnatal development, with expression gradually declining through adolescence and into adulthood (Gholizadeh et al., 2015; Till et al., 2015). Recent evidence highlights the critical role of temporally regulated *Fmr1* expression for proper microglial function during postnatal development (Hooshmandi et al., 2025). Indeed, early postnatal downregulation of *Fmr1* specifically in microglia was found to lead to reduced arborization, increased phagocytic activity, and behavioral impairments later in life, particularly in females, suggesting long-lasting effects of early microglial FMRP deficiency on brain homeostasis (Hooshmandi et al., 2025). Interestingly, the impact of microglial FMRP loss varies.

depending on the timing of its downregulation, with more pronounced effects observed when it occurs during early postnatal life, coinciding with peak FMRP expression in microglia. In addition to microglia, astrocytes have been implicated in the pathogenesis of rodent models of syndromic ASD, including FXS (Talvio and Castren, 2023).

For example, FMRP deficiency in astrocytes significantly impacts cortical excitability, synaptic transmission, and glutamate uptake, contributing to FXS-like behavioral phenotypes in conditional *Fmr1* knockout models (Higashimori et al., 2016; Jin et al., 2021). Increased GFAP expression - an indicator of astrocyte reactivity - has also reported in various brain regions, including the striatum, hippocampus, cortex, and cerebellum of adult *Fmr1* knockout mice (Lee et al., 2019; Pacey et al., 2015; Yuskaitis et al., 2010). In our study, we found a significant increase in the number of GFAP-positive cells in the CA1 and DG subregions of the hippocampus. Although glial cells might be particularly susceptible to early FMRP deficiency, potentially undergoing long-lasting structural and functional alterations, region-specific responses to local perturbations might also emerge over time. Indeed, microglia cells and astrocytes, which are continuously exposed to a dynamic microenvironment throughout life, adapt their transcriptional and functional states to specific developmental and various disease-related demands (Depp et al., 2025). In our study, all analyses were conducted in young adult *Fmr1-*$^{\Delta}$*exon 8* rats, a developmental stage at which several synaptic, neurotransmission, and behavioral phenotypes associated with *Fmr1* deficiency are already established (Golden et al., 2019; Jawaid et al., 2018; Tian et al., 2017); for a review, see also (Bostrom et al., 2016). Nevertheless, any relationship between the observed cellular changes and potential (dys-)functional or behavioral phenotypes should be interpreted with caution.

The morphological and numerical alterations observed in glial cells, in the absence of overt cytokine responses, suggest the existence of non-inflammatory cellular remodeling mechanisms that warrant further investigation.

Emerging evidence highlights an important role for lamins in regulating brain development and aging. Of interest, lamin defects have been linked to glia dysfunctions in age-related neurodegenerative disorders, such as Alzheimer's disease (Koufi et al., 2023). Lamin B1, a type V nuclear intermediate filament, forms a supportive mesh at the nuclear periphery and interacts with numerous proteins to regulate nuclear architecture, chromatin organization, transcriptional programs, neurogenesis, and cellular mechanics (de Leeuw et al., 2018). Dysregulation of Lamin B1 levels has been shown to exert distinct, age-dependent effects in the brain. Overexpression of Lamin B1 in the mouse brain has been associated with age-dependent astrocyte activation, as well as myelin abnormalities and neuronal activity defects (Heng et al., 2013; Ratti et al., 2021; Rolyan et al., 2015). Conversely, its downregulation contributes to age-related alterations in hippocampal neurogenesis and mood dysregulation (Bedrosian et al., 2021; Mahajani et al., 2017). In line with these findings, increased astrogenesis in the CA1 subfield of the hippocampus during postnatal development has been linked to autistic-like behaviors in mice through enhanced inhibitory synaptic transmission onto pyramidal neurons (J. Chen et al., 2022b). Furthermore, Matias et al. (2022) identified Lamin B1 loss and nuclear morphology alterations as hallmarks of the hippocampus of aged mice and humans, as well as of senescent CA1 astrocytes in vitro (Matias et al., 2022). Consistently, reduced Lamin B1 expression has been reported in GFAP-positive astrocytes within the substantia nigra pars compacta in Parkinsonian brains, but not in neighboring non-astrocytic populations, suggesting a selective vulnerability of astrocytes to lamin dysregulation in pathological conditions (Chinta et al., 2018).

To our knowledge, no studies have previously examined Lamin B1 dysregulation in FXS or related neurodevelopmental disorders. Here, we report for the first time a general reduction in Lamin B1 protein levels in the hippocampus of *Fmr1-*$^{\Delta}$*exon 8* rats. This decline is accompanied by

an increased percentage of dysmorphic nuclei, especially in astrocytes and microglia in the CA1 subfield of the hippocampus, a critical area for acquisition and retrieval of recent and remote memories. Although behavioral outcomes were not assessed in the present study, the observed Lamin B1 and glial alterations localize to hippocampal subfields previously associated with memory impairments in *Fmr1-$^{\Delta}$exon 8* rats (Manduca et al., 2024; Schiavi et al., 2023). Whether Lamin B1 dysregulation directly contributes to cognitive or emotional alterations in this model remains to be determined.

Loss of Lamin B1 and associated nuclear abnormalities might constitute early pathological hallmarks in glial cells, contributing to the broader spectrum of glial dysfunction observed in FXS and potentially other neurodevelopmental disorders.

Although a direct mechanistic link between *Fmr1* deficiency and Lamin B1 has not been established in FXS, alterations of nuclear lamina integrity have been described in Fragile X-associated tremor/ataxia syndrome (FXTAS), a neurodegenerative disorder also caused by a CGG-repeat expansion in the 5′ UTR of the FMR1 gene on the X-chromosome. In FXTAS, Lamin B1 ring disruption and aggregate formation have indeed been reported (Hoem et al., 2019), suggesting that the association described here may reflect a convergence between FMRP-dependent mechanisms, nuclear lamina integrity, and dysregulation of the hippocampal mechano-environment. These findings highlight important directions for future mechanistic investigation.

Supporting this view, previous studies have demonstrated that nuclear lamina reorganization, including Lamin B1 downregulation, is required for subnuclear gene repositioning and the activation of transcriptional programs during hippocampal neuron maturation (Noguchi et al., 2021). Such nuclear adaptations may be particularly relevant in glial cells, which exhibit high functional diversity and play a central role in maintaining tissue homeostasis (Allen and Lyons, 2018). Future studies should therefore investigate whether similar lamina-dependent mechanisms operate in glial cells, both during their maturation and in response to microenvironmental changes driven by FMRP deficiency.

In addition, components of the nuclear lamina, such as Lamin B1, serve as critical mediators for transmission of mechanical forces into the nucleus (Chen et al., 2015; Skinner and Johnson, 2017), linking cytoskeletal dynamics to chromatin organization and gene regulation. Whether the nuclear abnormalities observed here are mechanistically related to the glial morphological alterations described remains unknown, as does the extent to which Lamin B1 contributes to these processes. The potential bidirectional interplay between glial remodeling and nuclear architecture thus represents an important avenue for future investigation.

Finally, FMRP deficiency has been reported to perturb neurogenic programs from early stages of differentiation, potentially favoring glial fate specification (D'Antoni et al., 2024). In this context, the increased number of GFAP-positive cells in the hippocampus of *Fmr1-$^{\Delta}$exon* 8 rats may reflect such an imbalance. However, the precise interplay between FMRP and Lamin B1 in regulating neurogenesis and gliogenesis remains largely unexplored. This question may be particularly relevant in the adult hippocampus, a brain region that retains neurogenic potential throughout life (Toda et al., 2019).

Overall, the present findings identify Lamin B1 and nuclear architecture as previously unexplored cellular features in hippocampal glia in a rat model of FXS, providing a framework for future mechanistic studies without implying direct causality. Elucidating the developmental origins and functional significance of Lamin B1 downregulation will require multi-level approaches spanning molecular, cellular, and circuit-level analyses. Such studies will be essential to determine how FMRP-dependent pathways may influence Lamin B1 regulation and glial function in the context of FXS and ASD-related disorders, and may ultimately reveal novel molecular targets for intervention.

CRediT authorship contribution statement

Alessandro Rava: Writing – original draft, Data curation, Conceptualization. **Alessandro Feo:** Writing – review & editing, Investigation, Formal analysis, Data curation. **Giulia Bagnato:** Writing – review & editing, Methodology, Formal analysis, Data curation. **Valentina D'Oria:** Methodology. **Marco Pezzullo:** Methodology. **Stefania Petrini:** Writing – review & editing, Supervision, Methodology. **Valeria Buzzelli:** Writing – review & editing, Investigation, Formal analysis. **Fabrizio Ascone:** Writing – review & editing, Investigation, Formal analysis. **Melania Di Trapano:** Writing – review & editing, Investigation, Formal analysis. **Barbara Peruzzi:** Writing – review & editing, Writing – original draft, Supervision, Formal analysis, Data curation, Conceptualization. **Viviana Trezza:** Writing – review & editing, Writing – original draft, Project administration, Methodology, Investigation, Funding acquisition, Data curation, Conceptualization.

Funding

This work was supported by Jerome Lejeune Foundation Research grant #2209 - GRT-2023 A (VT), by PNRR– M4 C2 I1.1 -PRIN 2022CZTZ87- CUP F53D23006660006 - Dissecting the pharmacological mechanisms underlying the therapeutic potential of phytocannabinoids in autism- funded by European Union – NextGenerationEU (VT), and by European Union - Next Generation EU - National Recovery and Resilience Plan (NRRP) - Mission 6 - Component 2 - Investment 2.1. Strengthening and enhancing biomedical research in the NHS_CALL 2023, project titled "Interactions between type-1 trace amine receptors and metabotropic glutamate receptors in the pathophysiology and treatment of stress-related disorders and neurodevelopmental disorders" (PNRR-MCNT1–2023-12378320 to VT). The project was partly supported also by Rome Technopole, PNRR grant M4- C2-Inv. 1.5 -CUP F83B22000040006 to VT. In particular, the Western blot experiments were funded by Rome Technopole.

Declaration of competing interest

The authors declare no competing interests.

Appendix A. Supplementary data

Supplementary data to this article can be found online at https://doi.org/10.1016/j.nbd.2026.107304.

Data availability

Data will be made available on request.

References

Alkadhi, K.A., 2019. Cellular and molecular differences between area CA1 and the dentate gyrus of the Hippocampus. Mol. Neurobiol. 56 (9), 6566–6580. https://doi.org/10.1007/s12035-019-1541-2.

Allen, N.J., Lyons, D.A., 2018. Glia as architects of central nervous system formation and function. Science 362 (6411), 181–185. https://doi.org/10.1126/science.aat0473.

Ashwood, P., Krakowiak, P., Hertz-Picciotto, I., Hansen, R., Pessah, I., Van de Water, J., 2011. Elevated plasma cytokines in autism spectrum disorders provide evidence of immune dysfunction and are associated with impaired behavioral outcome. Brain Behav. Immun. 25 (1), 40–45. https://doi.org/10.1016/j.bbi.2010.08.003.

Bagni, C., Zukin, R.S., 2019. A synaptic perspective of fragile X syndrome and autism Spectrum disorders. Neuron 101 (6), 1070–1088. https://doi.org/10.1016/j.neuron.2019.02.041.

Basilico, B., Pagani, F., Grimaldi, A., Cortese, B., Di Angelantonio, S., Weinhard, L., Gross, C., Limatola, C., Maggi, L., Ragozzino, D., 2019. Microglia shape presynaptic properties at developing glutamatergic synapses. Glia 67 (1), 53–67. https://doi.org/10.1002/glia.23508.

Bedrosian, T.A., Houtman, J., Eguiguren, J.S., Ghassemzadeh, S., Rund, N., Novaresi, N. M., Hu, L., Parylak, S.L., Denli, A.M., Randolph-Moore, L., Namba, T., Gage, F.H., Toda, T., 2021. Lamin B1 decline underlies age-related loss of adult hippocampal neurogenesis. EMBO J. 40 (3), e105819. https://doi.org/10.15252/embj.2020105819.

Berry-Kravis, E.M., Lindemann, L., Jonch, A.E., Apostol, G., Bear, M.F., Carpenter, R.L., Crawley, J.N., Curie, A., Des Portes, V., Hossain, F., Gasparini, F., Gomez-Mancilla, B., Hessl, D., Loth, E., Scharf, S.H., Wang, P.P., Von Raison, F., Hagerman, R., Spooren, W., Jacquemont, S., 2018. Drug development for neurodevelopmental disorders: lessons learned from fragile X syndrome. Nat. Rev. Drug Discov. 17 (4), 280–299. https://doi.org/10.1038/nrd.2017.221.

Bhandari, K., Kanodia, H., Donato, F., Caroni, P., 2024. Selective vulnerability of the ventral hippocampus-prelimbic cortex axis parvalbumin interneuron network underlies learning deficits of fragile X mice. Cell Rep. 43 (5), 114124. https://doi.org/10.1016/j.celrep.2024.114124.

Bilousova, T.V., Dansie, L., Ngo, M., Aye, J., Charles, J.R., Ethell, D.W., Ethell, I.M., 2009. Minocycline promotes dendritic spine maturation and improves behavioural performance in the fragile X mouse model. J. Med. Genet. 46 (2), 94–102. https://doi.org/10.1136/jmg.2008.061796.

Blandin, K.J., Narvaiz, D.A., Sullens, D.G., Womble, P.D., Hodges, S.L., Binder, M.S., Faust, A., Nguyen, P.H., Pranske, Z.J., Lugo, J.N., 2024. A two-hit approach inducing flurothyl seizures in Fmr1 knockout mice impacts anxiety and repetitive Behaviors. Brain Sci. 14 (9). https://doi.org/10.3390/brainsci14090892.

Bostrom, C., Yau, S.Y., Majaess, N., Vetrici, M., Gil-Mohapel, J., Christie, B.R., 2016. Hippocampal dysfunction and cognitive impairment in fragile-X syndrome. Neurosci. Biobehav. Rev. 68, 563–574. https://doi.org/10.1016/j.neubiorev.2016.06.033.

Broers, J.L., Machiels, B.M., Kuijpers, H.J., Smedts, F., van den Kieboom, R., Raymond, Y., Ramaekers, F.C., 1997. A- and B-type lamins are differentially expressed in normal human tissues. Histochem. Cell Biol. 107 (6), 505–517. https://doi.org/10.1007/s004180050138.

Caffino, L., Verheij, M.M.M., Roversi, K., Targa, G., Mottarlini, F., Popik, P., Nikiforuk, A., Golebiowska, J., Fumagalli, F., Homberg, J.R., 2020. Hypersensitivity to amphetamine's psychomotor and reinforcing effects in serotonin transporter knockout rats: glutamate in the nucleus accumbens. Br. J. Pharmacol. 177 (19), 4532–4547. https://doi.org/10.1111/bph.15211.

Carbone, E., Buzzelli, V., Manduca, A., Leone, S., Rava, A., Trezza, V., 2023. Maternal immune activation induced by prenatal lipopolysaccharide exposure leads to Long-lasting autistic-like social, cognitive and immune alterations in male Wistar rats. Int. J. Mol. Sci. 24 (4). https://doi.org/10.3390/ijms24043920.

Chen, B., Co, C., Ho, C.C., 2015. Cell shape dependent regulation of nuclear morphology. Biomaterials 67, 129–136. https://doi.org/10.1016/j.biomaterials.2015.07.017.

Chen, J., Ma, X.L., Zhao, H., Wang, X.Y., Xu, M.X., Wang, H., Yang, T.Q., Peng, C., Liu, S. S., Huang, M., Zhou, Y.D., Shen, Y., 2022b. Increasing astrogenesis in the developing hippocampus induces autistic-like behavior in mice via enhancing inhibitory synaptic transmission. Glia 70 (1), 106–122. https://doi.org/10.1002/glia.24091.

Chen, Y.S., Guo, L., Han, M., Zhang, S.M., Chen, Y.Q., Zou, J., Bai, S.Y., Cheng, G.R., Zeng, Y., 2022a. Cerebellum neuropathology and motor skill deficits in fragile X syndrome. Int. J. Dev. Neurosci. 82 (7), 557–568. https://doi.org/10.1002/jdn.10217.

Chinta, S.J., Woods, G., Demaria, M., Rane, A., Zou, Y., McQuade, A., Rajagopalan, S., Limbad, C., Madden, D.T., Campisi, J., Andersen, J.K., 2018. Cellular senescence is induced by the environmental neurotoxin paraquat and contributes to neuropathology linked to Parkinson's disease. Cell Rep. 22 (4), 930–940. https://doi.org/10.1016/j.celrep.2017.12.092.

Colonna, M., Butovsky, O., 2017. Microglia function in the central nervous system during health and neurodegeneration. Annu. Rev. Immunol. 35, 441–468. https://doi.org/10.1146/annurev-immunol-051116-052358.

D'Antoni, S., Spatuzza, M., Bonaccorso, C.M., Catania, M.V., 2024. Role of fragile X messenger ribonucleoprotein 1 in the pathophysiology of brain disorders: a glia perspective. Neurosci. Biobehav. Rev. 162, 105731. https://doi.org/10.1016/j.neubiorev.2024.105731.

Depp, C., Doman, J.L., Hingerl, M., Xia, J., Stevens, B., 2025. Microglia transcriptional states and their functional significance: context drives diversity. Immunity 58 (5), 1052–1067. https://doi.org/10.1016/j.immuni.2025.04.009.

Dziembowska, M., Wlodarczyk, J., 2012. MMP9: a novel function in synaptic plasticity. Int. J. Biochem. Cell Biol. 44 (5), 709–713. https://doi.org/10.1016/j.biocel.2012.01.023.

Genovese, A.C., Butler, M.G., 2025. Systematic review: fragile X syndrome across the lifespan with a focus on genetics, neurodevelopmental, Behavioral and psychiatric associations. Genes (Basel) 16 (2). https://doi.org/10.3390/genes16020149.

Gholizadeh, S., Halder, S.K., Hampson, D.R., 2015. Expression of fragile X mental retardation protein in neurons and glia of the developing and adult mouse brain. Brain Res. 1596, 22–30. https://doi.org/10.1016/j.brainres.2014.11.023.

Gildea, H.K., Liddelow, S.A., 2025. Mechanisms of astrocyte aging in reactivity and disease. Mol. Neurodegener. 20 (1), 21. https://doi.org/10.1186/s13024-025-00810-7.

Golden, C.E.M., Breen, M.S., Koro, L., Sonar, S., Niblo, K., Browne, A., Burlant, N., Di Marino, D., De Rubeis, S., Baxter, M.G., Buxbaum, J.D., Harony-Nicolas, H., 2019. Deletion of the KH1 domain of Fmr1 leads to transcriptional alterations and attentional deficits in rats. Cereb. Cortex 29 (5), 2228–2244. https://doi.org/10.1093/cercor/bhz029.

Green, T.R.F., Murphy, S.M., Rowe, R.K., 2022. Comparisons of quantitative approaches for assessing microglial morphology reveal inconsistencies, ecological fallacy, and a need for standardization. Sci. Rep. 12 (1), 18196. https://doi.org/10.1038/s41598-022-23091-2.

Haberl, M.G., Zerbi, V., Veltien, A., Ginger, M., Heerschap, A., Frick, A., 2015. Structural-functional connectivity deficits of neocortical circuits in the Fmr1 (−/y) mouse model of autism. Sci. Adv. 1 (10), e1500775. https://doi.org/10.1126/sciadv.1500775.

Heng, M.Y., Lin, S.T., Verret, L., Huang, Y., Kamiya, S., Padiath, Q.S., Tong, Y., Palop, J. J., Huang, E.J., Ptacek, L.J., Fu, Y.H., 2013. Lamin B1 mediates cell-autonomous neuropathology in a leukodystrophy mouse model. J. Clin. Invest. 123 (6), 2719–2729. https://doi.org/10.1172/JCI66737.

Higashimori, H., Schin, C.S., Chiang, M.S., Morel, L., Shoneye, T.A., Nelson, D.L., Yang, Y., 2016. Selective deletion of Astroglial FMRP dysregulates glutamate transporter GLT1 and contributes to fragile X syndrome phenotypes in vivo. J. Neurosci. 36 (27), 7079–7094. https://doi.org/10.1523/JNEUROSCI.1069-16.2016.

Hodges, J.L., Yu, X., Gilmore, A., Bennett, H., Tjia, M., Perna, J.F., Chen, C.C., Li, X., Lu, J., Zuo, Y., 2017b. Astrocytic Contributions to synaptic and learning abnormalities in a mouse model of fragile X syndrome. Biol. Psychiatry 82 (2), 139–149. https://doi.org/10.1016/j.biopsych.2016.08.036.

Hodges, S.L., Nolan, S.O., Taube, J.H., Lugo, J.N., 2017a. Adult Fmr1 knockout mice present with deficiencies in hippocampal interleukin-6 and tumor necrosis factor-alpha expression. Neuroreport 28 (18), 1246–1249. https://doi.org/10.1097/WNR.0000000000000905.

Hodges, S.L., Nolan, S.O., Tomac, L.A., Muhammad, I.D.A., Binder, M.S., Taube, J.H., Lugo, J.N., 2020. Lipopolysaccharide-induced inflammation leads to acute elevations in pro-inflammatory cytokine expression in a mouse model of fragile X syndrome. Physiol. Behav. 215, 112776. https://doi.org/10.1016/j.physbeh.2019.112776.

Hoem, G., Bowitz Larsen, K., Overvatn, A., Brech, A., Lamark, T., Sjottem, E., Johansen, T., 2019. The FMRpolyGlycine protein mediates aggregate formation and toxicity independent of the CGG mRNA hairpin in a cellular model for FXTAS. Front. Genet. 10, 249. https://doi.org/10.3389/fgene.2019.00249.

Hooshmandi, M., Ho-Tieng, D., Lister, K.C., Cai, W., Wong, C., Brown, N., Fan, J., Hovhannisyan, V., Uttam, S., Prager-Khoutorsky, M., Sonenberg, N., Gkogkas, C.G., Khoutorsky, A., 2025. Postnatal downregulation of Fmr1 in microglia promotes microglial reactivity and causes behavioural alterations in female mice. Mol. Autism. 16 (1), 17. https://doi.org/10.1186/s13229-025-00648-2.

Hughes, H.K., Moreno, R.J., Ashwood, P., 2023. Innate immune dysfunction and neuroinflammation in autism spectrum disorder (ASD). Brain Behav. Immun. 108, 245–254. https://doi.org/10.1016/j.bbi.2022.12.001.

Ito, D., Imai, Y., Ohsawa, K., Nakajima, K., Fukuuchi, Y., Kohsaka, S., 1998. Microglia-specific localisation of a novel calcium binding protein, Iba1. Brain Res. Mol. Brain Res. 57 (1), 1–9. https://doi.org/10.1016/s0169-328x(98)00040-0.

Jawaid, S., Kidd, G.J., Wang, J., Swetlik, C., Dutta, R., Trapp, B.D., 2018. Alterations in CA1 hippocampal synapses in a mouse model of fragile X syndrome. Glia 66 (4), 789–800. https://doi.org/10.1002/glia.23284.

Jin, S.X., Higashimori, H., Schin, C., Tamashiro, A., Men, Y., Chiang, M.S.R., Jarvis, R., Cox, D., Feig, L., Yang, Y., 2021. Astroglial FMRP modulates synaptic signaling and behavior phenotypes in FXS mouse model. Glia 69 (3), 594–608. https://doi.org/10.1002/glia.23915.

Kalinowska, M., van der Lei, M.B., Kitiashvili, M., Mamcarz, M., Oliveira, M.M., Longo, F., Klann, E., 2022. Deletion of Fmr1 in parvalbumin-expressing neurons results in dysregulated translation and selective behavioral deficits associated with fragile X syndrome. Mol. Autism. 13 (1), 29. https://doi.org/10.1186/s13229-022-00509-2.

Kates, W.R., Abrams, M.T., Kaufmann, W.E., Breiter, S.N., Reiss, A.L., 1997. Reliability and validity of MRI measurement of the amygdala and hippocampus in children with fragile X syndrome. Psychiatry Res. 75 (1), 31–48. https://doi.org/10.1016/s0925-4927(97)00019-x.

Kim, Y., 2023. The impact of altered Lamin B1 levels on nuclear lamina structure and function in aging and human diseases. Curr. Opin. Cell Biol. 85, 102257. https://doi.org/10.1016/j.ceb.2023.102257.

Koncekova, J., Kotorova, K., Nemethova, M., Bona, M., Bonova, P., 2024. Effectiveness of remote ischaemic conditioning is not affected by hyper-inflammation in a rat model of stroke. Sci. Rep. 14 (1), 20750. https://doi.org/10.1038/s41598-024-71328-z.

Koufi, F.D., Neri, I., Ramazzotti, G., Rusciano, I., Mongiorgi, S., Marvi, M.V., Fazio, A., Shin, M., Kosodo, Y., Cani, I., Giorgio, E., Cortelli, P., Manzoli, L., Ratti, S., 2023. Lamin B1 as a key modulator of the developing and aging brain. Front. Cell. Neurosci. 17, 1263310. https://doi.org/10.3389/fncel.2023.1263310.

Lee, A.S., Azmitia, E.C., Whitaker-Azmitia, P.M., 2017. Developmental microglial priming in postmortem autism spectrum disorder temporal cortex. Brain Behav. Immun. 62, 193–202. https://doi.org/10.1016/j.bbi.2017.01.019.

Lee, F.H.F., Lai, T.K.Y., Su, P., Liu, F., 2019. Altered cortical cytoarchitecture in the Fmr1 knockout mouse. Mol. Brain 12 (1), 56. https://doi.org/10.1186/s13041-019-0478-8.

de Leeuw, R., Gruenbaum, Y., Medalia, O., 2018. Nuclear Lamins: thin filaments with major functions. Trends Cell Biol. 28 (1), 34–45. https://doi.org/10.1016/j.tcb.2017.08.004.

Lier, J., Streit, W.J., Bechmann, I., 2021. Beyond activation: characterizing microglial functional phenotypes. Cells 10 (9). https://doi.org/10.3390/cells10092236.

Lindenboim, L., Zohar, H., Worman, H.J., Stein, R., 2020. The nuclear envelope: target and mediator of the apoptotic process. Cell Death Discov. 6, 29. https://doi.org/10.1038/s41420-020-0256-5.

Liu, T., Zhang, L., Joo, D., Sun, S.C., 2017. NF-kappaB signaling in inflammation. Signal Transduct. Target. Ther. 2, 17023. https://doi.org/10.1038/sigtrans.2017.23.

Long, J., Li, H., Liu, Y., Liao, X., Tang, Z., Han, K., Chen, J., Zhang, H., 2024. Insights into the structure and function of the hippocampus: implications for the pathophysiology and treatment of autism spectrum disorder. Front. Psychol. 15, 1364858. https://doi.org/10.3389/fpsyt.2024.1364858.

Lopez-Ortiz, A.O., Eyo, U.B., 2024. Astrocytes and microglia in the coordination of CNS development and homeostasis. J. Neurochem. 168 (10), 3599–3614. https://doi.org/10.1111/jnc.16006.

Mahajani, S., Giacomini, C., Marinaro, F., De Pietri Tonelli, D., Contestabile, A., Gasparini, L., 2017. Lamin B1 levels modulate differentiation into neurons during embryonic corticogenesis. Sci. Rep. 7 (1), 4897. https://doi.org/10.1038/s41598-017-05078-6.

Manduca, A., Buzzelli, V., Rava, A., Feo, A., Carbone, E., Schiavi, S., Peruzzi, B., D'Oria, V., Pezzullo, M., Pasquadibisceglie, A., Polticelli, F., Micale, V., Kuchar, M., Trezza, V., 2024. Cannabidiol and positive effects on object recognition memory in an in vivo model of fragile X syndrome: obligatory role of hippocampal GPR55 receptors. Pharmacol. Res. 203, 107176. https://doi.org/10.1016/j.phrs.2024.107176.

Matias, I., Diniz, L.P., Damico, I.V., Araujo, A.P.B., Neves, L.D.S., Vargas, G., Leite, R.E. P., Suemoto, C.K., Nitrini, R., Jacob-Filho, W., Grinberg, L.T., Hol, E.M., Middeldorp, J., Gomes, F.C.A., 2022. Loss of Lamin-B1 and defective nuclear morphology are hallmarks of astrocyte senescence in vitro and in the aging human hippocampus. Aging Cell 21 (1), e13521. https://doi.org/10.1111/acel.13521.

Mestas, J., Hughes, C.C., 2004. Of mice and not men: differences between mouse and human immunology. J. Immunol. 172 (5), 2731–2738. https://doi.org/10.4049/jimmunol.172.5.2731.

Molnar, K., Keri, S., 2014. Bigger is better and worse: on the intricate relationship between hippocampal size and memory. Neuropsychologia 56, 73–78. https://doi.org/10.1016/j.neuropsychologia.2014.01.001.

Napier, M., Reynolds, K., Scott, A.L., 2023. Glial-mediated dysregulation of neurodevelopment in fragile X syndrome. Int. Rev. Neurobiol. 173, 187–215. https://doi.org/10.1016/bs.irn.2023.08.005.

Noguchi, A., Ito, K., Uosaki, Y., Ideta-Otsuka, M., Igarashi, K., Nakashima, H., Kakizaki, T., Kaneda, R., Uosaki, H., Yanagawa, Y., Nakashima, K., Arakawa, H., Takizawa, T., 2021. Decreased Lamin B1 levels affect gene positioning and expression in postmitotic neurons. Neurosci. Res. 173, 22–33. https://doi.org/10.1016/j.neures.2021.05.011.

Pacey, L.K., Doering, L.C., 2007. Developmental expression of FMRP in the astrocyte lineage: implications for fragile X syndrome. Glia 55 (15), 1601–1609. https://doi.org/10.1002/glia.20573.

Pacey, L.K., Guan, S., Tharmalingam, S., Thomsen, C., Hampson, D.R., 2015. Persistent astrocyte activation in the fragile X mouse cerebellum. Brain Behav. 5 (10), e00400. https://doi.org/10.1002/brb3.400.

Paolicelli, R.C., Sierra, A., Stevens, B., Tremblay, M.E., Aguzzi, A., Ajami, B., Amit, I., Audinat, E., Bechmann, I., Bennett, M., Bennett, F., Bessis, A., Biber, K., Bilbo, S., Blurton-Jones, M., Boddeke, E., Brites, D., Brone, B., Brown, G., C.,…Wyss-Coray, T., 2022. Microglia states and nomenclature: a field at its crossroads. Neuron 110 (21), 3458–3483. https://doi.org/10.1016/j.neuron.2022.10.020.

Parrott, J.M., Oster, T., Lee, H.Y., 2021. Altered inflammatory response in FMRP-deficient microglia. iScience 24 (11), 103293. https://doi.org/10.1016/j.isci.2021.103293.

Percie du Sert, N., Hurst, V., Ahluwalia, A., Alam, S., Avey, M.T., Baker, M., Browne, W. J., Clark, A., Cuthill, I.C., Dirnagl, U., Emerson, M., Garner, P., Holgate, S.T., Howells, D.W., Karp, N.A., Lazic, S.E., Lidster, K., MacCallum, C.J., Macleod, M., Pearl, E.J., Petersen, O.H., Rawle, F., Reynolds, P., Rooney, K., Sena, E.S., Silberberg, S.D., Steckler, T., Würbel, H., 2020. The ARRIVE guidelines 2.0: updated guidelines for reporting animal research. PLoS. Biol. 18 (7), e3000410. https://doi.org/10.1371/journal.pbio.3000410.

Pietropaolo, S., Goubran, M.G., Joffre, C., Aubert, A., Lemaire-Mayo, V., Crusio, W.E., Laye, S., 2014. Dietary supplementation of omega-3 fatty acids rescues fragile X phenotypes in Fmr1-ko mice. Psychoneuroendocrinology 49, 119–129. https://doi.org/10.1016/j.psyneuen.2014.07.002.

Ratti, S., Rusciano, I., Mongiorgi, S., Neri, I., Cappellini, A., Cortelli, P., Suh, P.G., McCubrey, J.A., Manzoli, L., Cocco, L., Ramazzotti, G., 2021. Lamin B1 accumulation's effects on autosomal dominant leukodystrophy (ADLD): induction of reactivity in the astrocytes. Cells 10 (10). https://doi.org/10.3390/cells10102566.

Rava, A., Buzzelli, V., Feo, A., Ascone, F., Di Trapano, M., Schiavi, S., Carbone, E., Pasquadibisceglie, A., Polticelli, F., Manduca, A., Trezza, V., 2025. Role of peroxisome proliferator-activated receptors alpha and gamma in mediating the beneficial effects of beta-caryophyllene in a rat model of fragile X syndrome. Prog. Neuro-Psychopharmacol. Biol. Psychiatry 136, 111234. https://doi.org/10.1016/j.pnpbp.2024.111234.

Rolyan, H., Tyurina, Y.Y., Hernandez, M., Amoscato, A.A., Sparvero, L.J., Nmezi, B.C., Lu, Y., Estecio, M.R., Lin, K., Chen, J., He, R.R., Gong, P., Rigatti, L.H., Dupree, J., Bayir, H., Kagan, V.E., Casaccia, P., Padiath, Q.S., 2015. Defects of lipid synthesis are linked to the age-dependent demyelination caused by Lamin B1 overexpression. J. Neurosci. 35 (34), 12002–12017. https://doi.org/10.1523/JNEUROSCI.1668-15.2015.

Rotschafer, S.E., Cramer, K.S., 2017. Developmental emergence of phenotypes in the auditory brainstem nuclei of Fmr1 knockout mice. eNeuro 4 (6). https://doi.org/10.1523/ENEURO.0264-17.2017.

Santana-Coelho, D., Lugo, J.N., 2023. Hippocampal upregulation of complement component C3 in response to lipopolysaccharide stimuli in a model of fragile-X syndrome. Curr. Issues Mol. Biol. 45 (11), 9306–9315. https://doi.org/10.3390/cimb45110582.

Sawicka, K., Hale, C.R., Park, C.Y., Fak, J.J., Gresack, J.E., Van Driesche, S.J., Kang, J.J., Darnell, J.C., Darnell, R.B., 2019. FMRP has a cell-type-specific role in CA1 pyramidal neurons to regulate autism-related transcripts and circadian memory. Elife 8. https://doi.org/10.7554/eLife.46919.

Schiavi, S., Carbone, E., Melancia, F., Buzzelli, V., Manduca, A., Campolongo, P., Pallottini, V., Trezza, V., 2022. Perinatal supplementation with omega-3 fatty acids corrects the aberrant social and cognitive traits observed in a genetic model of autism based on FMR1 deletion in rats. Nutr. Neurosci. 25 (5), 898–911. https://doi.org/10.1080/1028415X.2020.1819107.

Schiavi, S., Manduca, A., Carbone, E., Buzzelli, V., Rava, A., Feo, A., Ascone, F., Morena, M., Campolongo, P., Hill, M.N., Trezza, V., 2023. Anandamide and 2-arachidonoylglycerol differentially modulate autistic-like traits in a genetic model of autism based on FMR1 deletion in rats. Neuropsychopharmacology 48 (6), 897–907. https://doi.org/10.1038/s41386-022-01454-7.

Siniscalco, D., Schultz, S., Brigida, A.L., Antonucci, N., 2018. Inflammation and neuro-immune dysregulations in autism Spectrum disorders. Pharmaceuticals (Basel) 11 (2). https://doi.org/10.3390/ph11020056.

Skinner, B.M., Johnson, E.E., 2017. Nuclear morphologies: their diversity and functional relevance. Chromosoma 126 (2), 195–212. https://doi.org/10.1007/s00412-016-0614-5.

Sobo, J.M., Alagna, N.S., Sun, S.X., Wilson, K.L., Reddy, K.L., 2024. Lamins: the backbone of the nucleocytoskeleton interface. Curr. Opin. Cell Biol. 86, 102313. https://doi.org/10.1016/j.ceb.2023.102313.

Sun, C., Zhao, Y., Guo, L., Qiu, J., Peng, Q., 2025. The interplay between histone modifications and nuclear lamina in genome regulation. J. Genet. Genomics 52 (1), 24–38. https://doi.org/10.1016/j.jgg.2024.10.005.

Swift, J., Ivanovska, I.L., Buxboim, A., Harada, T., Dingal, P.C., Pinter, J., Pajerowski, J. D., Spinler, K.R., Shin, J.W., Tewari, M., Rehfeldt, F., Speicher, D.W., Discher, D.E., 2013. Nuclear Lamin-a scales with tissue stiffness and enhances matrix-directed differentiation. Science 341 (6149), 1240104. https://doi.org/10.1126/science.1240104.

Szpirer, C., 2020. Rat models of human diseases and related phenotypes: a systematic inventory of the causative genes. J. Biomed. Sci. 27 (1), 84. https://doi.org/10.1186/s12929-020-00673-8.

Takamori, Y., Hirahara, Y., Wakabayashi, T., Mori, T., Koike, T., Kataoka, Y., Tamura, Y., Kurebayashi, S., Kurokawa, K., Yamada, H., 2018. Differential expression of nuclear Lamin subtypes in the neural cells of the adult rat cerebral cortex. IBRO Rep. 5, 99–109. https://doi.org/10.1016/j.ibror.2018.11.001.

Talvio, K., Castren, M.L., 2023. Astrocytes in fragile X syndrome. Front. Cell. Neurosci. 17, 1322541. https://doi.org/10.3389/fncel.2023.1322541.

Tian, Y., Yang, C., Shang, S., Cai, Y., Deng, X., Zhang, J., Shao, F., Zhu, D., Liu, Y., Chen, G., Liang, J., Sun, Q., Qiu, Z., Zhang, C., 2017. Loss of FMRP impaired hippocampal Long-term plasticity and spatial learning in rats. Front. Mol. Neurosci. 10, 269. https://doi.org/10.3389/fnmol.2017.00269.

Till, S.M., Asiminas, A., Jackson, A.D., Katsanevaki, D., Barnes, S.A., Osterweil, E.K., Bear, M.F., Chattarji, S., Wood, E.R., Wyllie, D.J., Kind, P.C., 2015. Conserved hippocampal cellular pathophysiology but distinct behavioural deficits in a new rat model of FXS. Hum. Mol. Genet. 24 (21), 5977–5984. https://doi.org/10.1093/hmg/ddv299.

Toda, T., Parylak, S.L., Linker, S.B., Gage, F.H., 2019. The role of adult hippocampal neurogenesis in brain health and disease. Mol. Psychiatry 24 (1), 67–87. https://doi.org/10.1038/s41380-018-0036-2.

Tremblay, M.E., Zettel, M.L., Ison, J.R., Allen, P.D., Majewska, A.K., 2012. Effects of aging and sensory loss on glial cells in mouse visual and auditory cortices. Glia 60 (4), 541–558. https://doi.org/10.1002/glia.22287.

Vahabikashi, A., Adam, S.A., Medalia, O., Goldman, R.D., 2022. Nuclear lamins: structure and function in mechanobiology. APL Bioeng 6 (1), 011503. https://doi.org/10.1063/5.0082656.

Van Dijck, A., Barbosa, S., Bermudez-Martin, P., Khalfallah, O., Gilet, C., Martinuzzi, E., Elinck, E., Kooy, R.F., Glaichenhaus, N., Davidovic, L., 2020. Reduced serum levels of pro-inflammatory chemokines in fragile X syndrome. BMC Neurol. 20 (1), 138. https://doi.org/10.1186/s12883-020-01715-2.

Wang, X., Li, K., Guo, L., Liu, X., Guo, Y., Zhang, W., 2025. The influence of changes in microglia development on the plasticity of the developing visual cortex circuit in juvenile mice. Invest. Ophthalmol. Vis. Sci. 66 (4), 45. https://doi.org/10.1167/iovs.66.4.45.

Willemsen, R., Kooy, R.F., 2023. Mouse models of fragile X-related disorders. Dis. Model. Mech. 16 (2). https://doi.org/10.1242/dmm.049485.

Young, K., Morrison, H., 2018. Quantifying microglia morphology from photomicrographs of immunohistochemistry prepared tissue using ImageJ. J Vis Exp 136. https://doi.org/10.3791/57648.

Yu, K.H., Palmer, N., Fox, K., Prock, L., Mandl, K.D., Kohane, I.S., Prilutsky, D., 2020. The phenotypical implications of immune dysregulation in fragile X syndrome. Eur. J. Neurol. 27 (3), 590–593. https://doi.org/10.1111/ene.14146.

Yuskaitis, C.J., Beurel, E., Jope, R.S., 2010. Evidence of reactive astrocytes but not peripheral immune system activation in a mouse model of fragile X syndrome. Biochim. Biophys. Acta 1802 (11), 1006–1012. https://doi.org/10.1016/j.bbadis.2010.06.015.

Zhang, J., Hou, L., Klann, E., Nelson, D.L., 2009. Altered hippocampal synaptic plasticity in the FMR1 gene family knockout mouse models. J. Neurophysiol. 101 (5), 2572–2580. https://doi.org/10.1152/jn.90558.2008.

Zschaler, J., Schlorke, D., Arnhold, J., 2014. Differences in innate immune response between man and mouse. Crit. Rev. Immunol. 34 (5), 433–454.

Glossary

ASD *Autism spectrum disorder:*
CA1 *Cornu ammonis 1:*
DG *Dentate gyrus:*
Fmr1 *Fragile X messenger ribonucleoprotein 1:*
FMRP *Fragile X messenger ribonucleoprotein:*
FXS *Fragile X syndrome:*
GFAP *Glial fibrillar acidic protein:*
GL *granular layer:*

HL *hilus:*
Iba1 *Ionized calcium-binding adapter molecule 1:*
KO *Knockout:*
M *protein marker:*
MFI *Mean fluorescent intensity:*
ML *molecular layer:*
NF-κB *Nuclear factor-κB:*
PBS *Phosphate-buffered saline:*
PND *Postnatal day:*
SO *stratum oriens:*
SP *stratum pyramidale:*
SR *stratum radiatum:*
TBS *Tris-buffered saline:*
WT *Wild type:*